NASA TECHNICAL MEMORANDUM

NASA TM X-3397

NASA TM X-3397

PERFORMANCE OF A MULLITE REUSABLE SURFACE INSULATION SYSTEM IN A HYPERSONIC STREAM

L. Roane Hunt

Langley Research Center
Hampton, Va. 23665

NATIONAL AERONAUTICS AND SPACE ADMINISTRATION • WASHINGTON, D. C. • AUGUST 1976

1. Report No. NASA TM X-3397	2. Government Accession No.	3. Recipient's Catalog No.
4. Title and Subtitle PERFORMANCE OF A MULLITE REUSABLE SURFACE INSULATION SYSTEM IN A HYPERSONIC STREAM		5. Report Date August 1976 6. Performing Organization Code
7. Author(s) L. Roane Hunt		8. Performing Organization Report No. L-10861
9. Performing Organization Name and Address NASA Langley Research Center Hampton, Va. 23665		10. Work Unit No. 506-17-22-01 11. Contract or Grant No.
12. Sponsoring Agency Name and Address National Aeronautics and Space Administration Washington, D.C. 20546		13. Type of Report and Period Covered Technical Memorandum 14. Sponsoring Agency Code
15. Supplementary Notes		

16. Abstract

The thermal and structural performance of a large panel of mullite reusable surface insulation (RSI) tiles was determined by a series of aerothermal tests in the Langley 8-foot high-temperature structures tunnel. The test panel was designed to represent a portion of the surface structure on a space-shuttle-orbiter fuselage along a 1150 K isotherm with the mullite tile system bonded directly to the primary structure. Aerothermal tests were conducted at a free-stream Mach number of 6.7, a total temperature of 1880 K, a unit Reynolds number of 4.6×10^6 per meter, and a dynamic pressure of 62 kPa. The thermal response of the mullite tile was as predicted, and the bond-line temperature did not exceed the design level of 570 K during a typical entry-heat cycle. Geometric irregularities of the tile gaps affected the tile edge temperatures when exposed to hypersonic flow. The tile coating demonstrated good toughness to particle impacts, but the coating cracked and flaked with thermal cycles. The gap filler of woven silica fibers appeared to hinder flow penetration into the gaps and withstood the flow shear of the present tests.

17. Key Words (Suggested by Author(s)) Hypersonic flow Thermal protection Surface insulation	18. Distribution Statement Unclassified – Unlimited Subject Category 18		
19. Security Classif. (of this report) Unclassified	20. Security Classif. (of this page) Unclassified	21. No. of Pages 37	22. Price* $3.75

*For sale by the National Technical Information Service, Springfield, Virginia 22161

PERFORMANCE OF A MULLITE REUSABLE SURFACE INSULATION SYSTEM IN A HYPERSONIC STREAM

L. Roane Hunt
Langley Research Center

SUMMARY

The thermal and structural performance of a large panel of mullite reusable surface insulation (RSI) tiles was determined by a series of aerothermal tests in the Langley 8-foot high-temperature structures tunnel. The test panel was designed to represent a portion of the surface structure on a space-shuttle-orbiter fuselage along a 1150 K isotherm with the mullite tile system bonded directly to the primary structure. Aerothermal tests were conducted at a free-stream Mach number of 6.7, a total temperature of 1880 K, a unit Reynolds number of 4.6×10^6 per meter, and a dynamic pressure of 62 kPa. The thermal response of the mullite tile was as predicted, and the bond-line temperature did not exceed the design level of 570 K during a typical entry-heat cycle. Geometric irregularities of the tile gaps affected the tile edge temperatures when exposed to hypersonic flow. The tile coating demonstrated good toughness to particle impacts, but the coating cracked and flaked with thermal cycles. The gap filler of woven silica fibers appeared to hinder flow penetration into the gaps and withstood the flow shear of the present tests.

INTRODUCTION

The requirement of reusability of thermal protection systems (TPS) of the current shuttle and future space transports has placed major emphasis on the development of lightweight TPS with good durability. (See refs. 1 and 2.) A primary candidate TPS is the reusable surface insulation (RSI) concept which consists of low-density ceramic tiles bonded to primary structure. Large tile arrays have been tested in radiant heating facilities, and small arrays have also been tested in arc-heated wind tunnels. A thorough evaluation, however, should include aerothermal tests on large tile arrays where flow effects of a thick boundary layer including aerodynamic shear are combined with the aerodynamic heat load. In support of this need, the Langley Research Center initiated an extensive testing program for assessing the thermal and structural performance of large RSI and metallic TPS concepts in an aerothermal environment. (See refs. 3, 4, and 5.) As part of this program, aerothermal cyclic tests were conducted on a TPS concept incorporating mullite RSI, which was an early contender as a space-shuttle TPS material. Results of these tests are presented herein.

The test panel consisted of mullite tiles bonded to a titanium primary structure. Gaps between tiles were filled with strips of woven silica fibers. The primary structure was designed and fabricated by Rockwell International and the TPS was furnished by General Electric; the design represents a portion of the surface structure on a shuttle orbiter fuselage along a 1150 K isotherm. The panel was subjected to 21 thermal tests, in 9 of which both radiant heating and aerodynamic heating were combined to represent an entry temperature history. The other 12 thermal tests used only radiant heating at atmospheric pressure to expose the panel to additional temperature history cycles to demonstrate reuse capability. All tests were conducted in the Langley 8-foot high-temperature structures tunnel. For the aerodynamic heating tests free-stream Mach number was 6.7, total temperature was 1880 K, unit Reynolds number was 4.6×10^6 per meter, and dynamic pressure was 62 kPa.

SYMBOLS

M	Mach number
p	pressure, Pa
q	dynamic pressure, Pa
R	unit Reynolds number, m^{-1}
T	temperature, K
t	time, s
α	angle of attack, deg
Δp	differential pressure load on test panel, Pa

Subscripts:

l	local flow
t	total
∞	free-stream flow

APPARATUS AND TEST

Panel

The test panel is shown in figures 1 and 2. It has overall dimensions of 91.4 by 137.2 by 20.3 cm and consists of an array of 24 RSI tiles bonded to a primary structure. The gaps between the tiles were filled with woven silica fibers. The tiles consist of mullite (MOD IA) insulation with a glass coating (SR-2) and are described in reference 6. Mullite is made of fibers from a mixture of oxides (77 percent alumina) rigidized by an alumina-boria-silica binder. The insulation and coating densities are 219 and 2160 kg/m^3, respectively. Each tile is nominally 22.9 cm square with a thickness of 3.24 cm. The coating thickness is 0.04 cm. The tiles are staggered in spanwise rows of two and are bonded to a strain isolator which is, in turn, bonded to the primary structure shown in detail by figure 2. The 0.76-cm-thick strain isolator is composed of silicone foam (PD-200). The adhesive is a silicone rubber (RTV 560). The skin and hat-section stiffeners of the primary structure are fabricated from 0.1-cm sheets of titanium. The stiffeners (fig. 2(b)) are riveted to the skin. The stiffened skin is attached to support channels by the stringers and clips made from 0.13-cm corrosion-resistant steel (fig. 2(c)). The unit masses of the TPS and primary-structure components are listed in table I.

The "omniweave" gap filler is illustrated in figure 3. The lower edge of the strips were bonded to the strain isolator, and the upper edges were designed to extend to within 0.2 cm of the top surface of the tile. However, the omniweave height varied considerably with many fibers extending above the tiles. (See fig. 1.) Also, additional loose fibers were placed in gaps where the omniweave did not reach the prescribed height. The panel was designed to have a 0.36-cm gap width, but actual measured widths varied from 0.13 to 0.43 cm as shown in figure 4(a). Also, the step height between tiles normal to the flow direction was as much as 0.2 cm even though the panel was designed to have level tiles. Relative step heights are indicated in figure 4(b) with rearward-facing steps shown negative. The alphanumeric system defined in figure 4 is used in subsequent sections to locate areas of interest.

Panel Instrumentation

Panel temperatures were recorded from thermocouples located on the tiles and the primary structure. The tile thermocouples were placed just under the coating on the center of tiles. Additional thermocouples were embedded in the omniweave gap filler. Many thermocouples were located on the structure skin, stiffeners, and stringers. The specific locations of thermocouples will be identified only for those for which results are presented, and the locations are given with the results in the section entitled "Results and Discussion."

In addition to measuring tile surface temperature with thermocouples, the surface temperature distribution was determined using a scanning infrared radiometer. Thermal radiation from the panel surface was monitored by a photovoltaic indium-antimonide detector which mechanically scanned the surface with a nominal spatial resolution of 1.3 cm in diameter when the panel is located in the test stream. For the present tests this system was sensitive to a temperature range from 650 K to 1400 K. The radiometer is described in references 5, 7, and 8.

Panel Holder

Aerothermal tests were performed using the sting-mounted panel holder shown in figure 5. The panel holder is a rectangular slab with a beveled leading edge and aerodynamic fences to provide uniform aerodynamic pressure and heat-transfer loading to the test-panel surface. A boundary-layer trip provides turbulent flow over the test surface. The flow calibration of the panel holder is described in reference 9. Tests are made using the panel holder pitched at angles to the test stream varying from 0° to 15°.

The test panel was installed in a 108- by 152-cm cutout of the panel holder with the surfaces of the test panel and panel holder flush. (See fig. 6.) The perimeter of the panel was sealed with silicone rubber. The panel was supported by longitudinal structural beams attached to the sidewalls of the cutout. The bottom of the cutout was covered by an access door providing a usable space 25 cm deep between the door and the test-panel surface for the panel and instrumentation. The space between the test panel and the door was vented to the low base pressure of the holder to provide differential pressure loading on the panel.

Facility

The tests were conducted in the Langley 8-foot high-temperature structures tunnel (HTST) shown schematically in figure 7. This facility is a hypersonic blowdown wind tunnel that uses the combustion products of methane and air as the test medium and operates at a nominal Mach number of 7, at total pressures between 3.4 and 24.1 MPa, and at nominal total temperatures between 1400 K and 2000 K. Corresponding free-stream unit Reynolds numbers are between 1×10^6 and 10×10^6 per meter. These conditions simulate the aerothermal flight environment at Mach 7 in the altitude range between 25 and 40 km. As indicated in figure 7, the panel holder is retained in the pod below the test chamber during facility startup and shutdown so that the panel is exposed only to the desired stream conditions.

Although the facility provides aerodynamic exposure times of up to 120 s, thermal exposure times can be extended indefinitely by means of a pair of retractable quartz-lamp radiant heaters located in the pod. These heaters and the entire test surface of the panel

holder are covered by a pair of acoustic baffles which protect the panel from potentially damaging acoustic disturbance and buffeting generated during facility startup and shutdown. Sketches of the radiant heaters and acoustic baffles are shown in figure 8. The sketches in figure 9 show the panel holder covered by the heaters during pretest and posttest conditions and also show the panel holder in test position with heaters retracted. Additional information pertaining to this equipment and the test facility may be found in references 7 and 9.

Test Procedure

The test panel was repeatedly exposed to surface temperature cycles typical of that illustrated in figure 10. The first part of the thermal cycles was accomplished by radiant heat and was characterized by a linear heatup period at 2 K/s to a surface temperature of about 1200 K followed by a constant-temperature period. After a brief 3- to 5-s delay required to retract the heaters and insert the panel into the stream, the second part of the thermal load was provided by aerodynamic heating where the test conditions were selected to sustain the preheat temperature. Thus, in this type of test, an entry thermal cycle which includes a short exposure to aerodynamic heating and pressure loads can be imposed upon the test panel. Additional thermal cycles were imposed upon the test panel where the entire thermal cycle was accomplished with the radiant heaters only. The design entry thermal cycle for the present test panel consisted of a 420-s heatup and a 1260-s period at a constant temperature of 1150 K. The total thermal cycle including the cooldown was 2100 s. The thermal cycles of the present tests were shorter in time and slightly higher in surface temperature than the design condition, but the important feature of these tests was the aerothermal, cyclic exposures.

Tests

The test panel was exposed to a total of 21 thermal cycles with 9 of these including the aerodynamic exposure. The sequence of tests and the test conditions are listed in table II. The heatup times were consistent between 330 to 390 s, but the constant-temperature times varied greatly between 30 s for test 3 (heater malfunction) and 1285 s for test 17. In general, the constant-temperature times varied because of unexpected delays in starting the wind tunnel. The radiant heating was maintained during these delays until the test stream was established. The nominal test condition for the aerodynamic heating period was a time t of 41 s, an angle of attack α of 15°, and a differential pressure Δp of 11.0 kPa. (The conditions of test 6 were unintentionally slightly different from the nominal conditions because α was 13° and Δp was 13.8 kPa.) The surface temperature histories for each aerodynamic heating test are presented in figure 11. Above each plot, the radiant-heat temperature and time are given. The time is the sum of the heatup and constant-temperature time given in table II. Also, the time for

insertion into the test stream and for retraction from the test stream is given in each plot. The shorter stream exposures of tests 6 and 16 were caused by facility malfunctions. Flow conditions for the aerodynamic heating tests are given in table III. Free-stream total temperature, unit Reynolds number, dynamic pressure, Mach number, and static pressure are given for each test. Also, the local unit Reynolds number, dynamic pressure, Mach number, and static pressure are given for each test. The local flow shear for these tests was about 0.27 kPa.

RESULTS AND DISCUSSION

Thermal Response

The thermal cycles imposed on the test panel were similar to the design thermal cycle, but all were for shorter time duration with the exception of test 17. During the radiant-heat phase of the thermal cycle, the thermal response of the panel was monitored by thermocouples only. When the radiant heaters were retracted, the surface temperature of the panel could be monitored by the infrared radiometer.

Temperature histories.- Thermal response through the thickness of the panel was calculated using the finite-difference thermal analysis of reference 10. The structural details of the skin and stiffener were represented by a two-dimensional theoretical model which included a radiant-heat exchange between the structure and a lower surface at ambient temperature. The thermal properties used in the analysis were obtained from reference 6.

The thermal response of the mullite TPS panel to the radiant-heat cycle of test 17 is representative of all radiant-heat cycles and is presented in figure 12. The experimental temperature histories of the mullite surface and the titanium skin are shown by the solid curves. Thermocouples were located in the middle of the tile (location F5) as shown in the inset. The surface temperature history closely followed the design thermal cycle shown by the long-dash—short-dash curve. The temperatures of the panel interior, shown by the dashed curves, were calculated using the experimental surface temperature history as an input. The skin temperature was predictable and the corresponding bondline temperature between the tile and the strain isolator did not exceed 570 K which was the design limit for the present panel. Therefore, at the midtile location, the panel performed under radiant-heat exposure as it was designed to perform.

A similar temperature history of the response of the panel during test 13 which included aerodynamic-heat exposure is presented in figure 13(a). Experimental temperature histories for the RSI surface and panel skin are shown by the solid curves. The predicted skin temperature (dashed curve) is in good agreement with the experiment. The aerodynamic heating portion of test 13, which covered a time period from 804 to 845 s,

is presented with an expanded time scale in figure 13(b). The additional experimental surface temperature data shown were obtained using the infrared radiometer. For the aerodynamic heating phase, the calculated surface temperatures (dashed curves) were obtained using the convective heating values from calibration tests presented in reference 9. The surface emissivities used for the radiometer and in the thermal analysis are presented in reference 8. The calculated surface temperature is in fair agreement with the temperature measured by the radiometer, but the temperature of the surface thermocouple was lower since it was embedded beneath the RSI coating. The skin temperature beneath the center of the tile was not affected by the relatively short aerodynamic-flow exposure, and no leakage through the panel perimeter was detected.

Surface temperatures.- An RSI-surface temperature distribution obtained from the infrared radiometer during a typical thermal cycle (test 13) is presented in figure 14. The data from the radiometer were reduced and presented on a computer graphic display. Areas of the panel surface were assigned colors as a function of temperature as identified by the color charts of each photograph. In figure 14(a) the surface temperature distribution for the entire panel is shown after the radiant heaters were retracted and before the panel was inserted into the test stream. The dashed lines represent the tile gap locations. These data were obtained while the panel temperature was decreasing rapidly. The radiometer sweep time from row 9 to row 1 was 2.9 s which corresponds to about a 75 K temperature drop at row 1 with respect to the temperatures that existed at the time the sweep began. Therefore, the indicated temperature distribution is slightly distorted but gives a general view of the hotter and cooler areas resulting from nonuniform radiant heating. Three hot areas above 1175 K are near locations D4, G7, and K6 and the surface temperature variation on some of the tiles in these areas is as much as 100 K. Although the uneven temperature distribution was not intentional it may be realistic of increased heating during entry flight in areas of protuberances or shock interference. In figure 14(b) a portion of the panel surface (from about row E to M and row 3 to 7) is shown where the panel is in the test stream at test times between 840 and 843 s. In the stream the panel surface temperature does not show any effect of the irregular preheat distribution. The RSI-tile surface temperature varied from about 1225 K to 1300 K. Temperatures above 1300 K were produced at the tile edges. However, at row K the tile edges were cool because of a rearward-facing step of 0.05 to 0.2 cm. (See fig. 4.) Just downstream of the cool edge the surface temperature was above 1300 K in spots apparently because of flow reattachment.

The irregular temperature distribution along the tile edges is also shown in figure 15 by a photograph obtained during the aerodynamic heating part of test 18. The photograph shows the natural glow of the hot panel. Hot tile edges were caused by tile-gap geometric irregularities such as forward-facing steps, wide gaps, and damaged spots. For example, the bright edges along row E were caused by forward-facing steps

as high as 0.08 cm. (See fig. 4.) Also the bright edges along row 7 between row I and K (shown also in fig. 14) were caused by the wide tile gap of about 0.37 cm. The bright spot near location J3 in both figures 14 and 15 is caused by a damaged tile edge. The longitudinal tile edges along row 6 between rows E and I appear to be lower in temperature in both figures 14 and 15 which suggests that this gap might have closed from tile thermal expansion thus allowing less local flow in the gap.

Gap filler.- The thermal performance of the omniweave gap filler is indicated to a limited degree in figure 16. The temperature histories for the tile surface (1) and skin (2) from figure 13(b) (aerodynamic heating portion of test 13) are presented along with the temperature histories of the skin under a gap (4) and thermocouples embedded at the top of the gap filler ((3), (5), (6), and (7)). The location of each thermocouple is shown in the plan-view inset and additional details are given in sections A-A and B-B. The embedded thermocouple in the omniweave gap filler (3) is typical of thermocouples (5), (6), and (7). Posttest inspection of the omniweave revealed that the thermocouples were located near the top but about 1 cm deep into the omniweave as shown in section A-A. At the end of the radiant-heat phase of test 13 at $t = 797$ s, three of the thermocouples in the gap filler were within 100 K of the temperature of the tile surface (1). The other gap thermocouple (7) was lower in temperature because it was probably embedded deeper into the omniweave. When the radiant heaters were retracted, the thermocouples in the omniweave did not cool as rapidly as the tile surface (1). After the panel was inserted into the stream at $t = 804$ s, the temperatures of the lateral-gap thermocouples changed only slightly. The slight differences between the temperature of thermocouples (3), (5), and (6) may have been caused by flow disturbance produced by the geometric irregularities of the tile gaps. (See fig. 4.) Apparently, the omniweave substantially prohibits flow penetration into the lateral gap to the depth of the thermocouples. The skin temperature was significantly higher beneath the gap (4) than it was under the tile (2) because of the superior insulative characteristics of the tile. The skin temperature beneath the gap (4) does not differentiate between the radiant heating and the 41 s of aerodynamic heating because the omniweave and thick strain isolator insulated the skin from transient heat loads.

Tile Damage Tolerance

During the test series, the tiles incurred considerable surface damage such as particle impact craters, coating cracks, tile flaking, and tile erosion. The overall appearance of the tile surface before test 4 and at the conclusion of test 21 is shown in figure 17. (The corner tile at location A1 of fig. 17(a) was damaged and replaced before the first test. The new tile is white because a different pigment was used in the coating.) In figure 17(b) some of the more extensive damaged areas are noted. Six damaged areas noted by "c" are large craters caused by particle impact which have been repaired with a ceramic cement. The particles which caused these craters were

debris left in the facility piping after system repairs. The four damaged areas noted by "f" were caused by tile flaking in areas where the coating cracked extensively, and the two areas noted by "e" are areas of erosion. The damaged areas are illustrated in more detail in subsequent figures.

Craters in the tile surface too small to be seen in figure 17 were produced during aerodynamic heating because the panel was bombarded by very small particles in the test stream. These small particles were produced by the spalling of an aluminum oxide coating from the facility combustor liner. There were about 40 craters of less than 0.4 cm in diameter in each tile, and evidence of numerous other impacts is indicated by marks on the tile surface as shown in figure 18. Damage of this type was much less extensive than that which resulted from tests of a LI-1542 RSI tile in this facility. (See ref. 4.) Resistance of the mullite tile to the small impacting particles indicates that the toughness of the tile coating with respect to surface abrasion was good.

The tile coating failed from the thermal cycles of the present tests. The failure progressed from crazing of the coating to the flaking of large segments of the coating which exposed the mullite insulation. The coating failure is illustrated in figure 19 where photographs of a tile taken after three successive tests are presented. After test 19 (fig. 19(a)), the coating was cracked and buckled in the area enclosed by the dashed lines. (The center of the tile was repaired after impact damage which occurred during test 16.) After test 20 (fig. 19(b)), segments of the coating are missing. In figure 19(c) the same tile is shown after test 21, and more of the coating is missing. The cracks in the tile coating could generally be seen by the naked eye, but they were enhanced in figure 19(c) by wetting the coating with a volatile solvent. The pieces that flaked were segments of coating isolated by the crack pattern. The inplane failure line was beneath the coating in the weaker mullite insulation. Apparently the coated mullite tile did not withstand the thermal cycles of the present test because of the mismatch of thermal expansion characteristics of the mullite insulation and the coating.

An extreme case of flaking occurred during test 6, the first test which included aerodynamic exposure. A posttest photograph is presented in figure 20 which shows the damaged tile with a large hole about 1 cm deep. The tile had been severely cracked during the earlier thermal cycles. In fact, the front edge of the crack surface had a forward-facing step of about 0.04 cm before test 6. In this case, the cracks were through the coating and apparently penetrated deep into the mullite insulation so that the flake actually contained a large piece of insulation as well as the coating. The flake was dislodged during the wind-tunnel startup or model insertion into the test stream because the flake was already blown clear at the first view of the panel in the test position. The damaged area was repaired with a ceramic cement and the tests continued.

Tile erosion in the present tests occurred primarily on forward-facing steps between tiles as illustrated in figure 21. The downstream tile at lateral row E between

longitudinal rows 4 and 6 had a forward-facing step of 0.05 to 0.08 cm (fig. 4(b)). In figure 21(a) a portion of the panel along row E is shown after test 13 where the panel had experienced three aerodynamic exposures for a total of 99 s without evidence of erosion. The same area after test 21 and 304 s of aerodynamic exposure is shown in figure 21(b). Considerable erosion occurred at location E5, apparently because the raised tile edges were more susceptible to the foreign-particle impacts discussed earlier which evidently broke the coating and caused erosion of the insulation and further flaking of coating.

The omniweave gap filler remained in position within the gaps for the entire test series although the top edge in some locations was frayed from the flow shear. Following the tests, a portion of tile and strain isolator was removed to examine the omniweave and the lower portion of the tile gap along row 7 and row E as shown in figure 22. The top of the omniweave along row 7, which is parallel to the flow, has been eroded particularly near the intersection of rows 7 and E where the top of the remaining omniweave is only 0.8 cm from the top of the tile. However, it appears that the omniweave along the lateral row E did not erode. Also, the strain isolator below the omniweave showed no sign of deterioration. In some of the gaps, there was an apparent shrinkage in the width of the omniweave probably caused by the cyclic compression of the omniweave from the tile expansion during each thermal cycle. Overall, the omniweave demonstrated good durability as it withstood the flow shear of the present tests.

CONCLUDING REMARKS

A large panel of mullite reusable surface insulation (RSI) tiles was subjected to a total of 21 cyclic heating tests using radiant and aerodynamic heating in the Langley 8-foot high-temperature structures tunnel to assess its thermal and structural performance. The test panel was designed to represent a portion of the surface structure on a space-shuttle-orbiter fuselage along a 1150 K isotherm. Aerothermal tests were conducted at a free-stream Mach number of 6.7, a total temperature of 1880 K, a unit Reynolds number of 4.6×10^6 per meter, and a dynamic pressure of 62 kPa.

The mullite RSI tiles performed as designed for thermal protection of the primary structure; that is, the bond-line temperature did not exceed the design level of 570 K during a typical entry heat cycle. The gap width variation between tiles and misalinement of tile height affected tile edge temperatures when exposed to hypersonic flow. The tile coating demonstrated good toughness to particle impacts, but the coating cracked and flaked with thermal cycles. The omniweave gap filler appeared to hinder flow penetration into the gaps and withstood the flow shear of the present tests.

Langley Research Center
National Aeronautics and Space Administration
Hampton, Va. 23665
June 10, 1976

REFERENCES

1. Anderson, Roger A.; Brooks, William A., Jr.; Leonard, Robert W.; and Malz, Joseph: Structures – A Technology Overview. Astronaut. & Aeronaut., vol. 9, no. 2, Feb. 1971, pp. 38-47.

2. Love, Eugene S.: Advanced Technology and the Space Shuttle. Astronaut. & Aeronaut., vol. II, no. 2, Feb. 1973, pp. 30-66.

3. Bohon, Herman L.; Sawyer, J. Wayne; Hunt, L. Roane; and Weinstein, Irving: Performance of Full Size Metallic and RSI Thermal Protection Systems in a Mach 7 Environment. AIAA Paper No. 75-800, May 1975.

4. Hunt, L. Roane; Shideler, John L.; and Weinstein, Irving: Performance of LI-1542 Reusable Surface Insulation System in a Hypersonic Stream. NASA TN D-8150, 1976.

5. Deveikis, William D.; Miserentino, Robert; Weinstein, Irving; and Shideler, John L.: Aerothermal Performance and Structural Integrity of a René 41 Thermal Protection System at Mach 6.6. NASA TN D-7943, 1975.

6. Tanzilli, Richard A., ed.: Development of an External Ceramic Insulation for the Space Shuttle Orbiter. NASA CR-112038, 1972.

7. Deveikis, William D.; Bruce, Walter E., Jr.; and Karns, John R.: Techniques for Aerothermal Tests of Large, Flightweight Thermal Protection Panels in a Mach 7 Wind Tunnel. NASA TM X-71983, 1974.

8. Kantsios, Andronicos G.; Edwards, S. Franklin; and Dicus, Dennis L.: Spectral and Total Normal Emittance of Reusable Surface Insulation Materials. Symposium on Reusable Surface Insulation for Space Shuttle, Vol. I, NASA TM X-2719, 1973, pp. 327-347.

9. Deveikis, William D.; and Hunt, L. Roane: Loading and Heating of a Large Flat Plate at Mach 7 in the Langley 8-Foot High-Temperature Structures Tunnel. NASA TN D-7275, 1973.

10. Martin Interactive Thermal Analyzer System – Version 1.0. User's Manual. MDS-SPLPD-71-FD238 (REV 3), Martin Marietta Corp., Mar. 1972.

TABLE I.- UNIT MASSES OF MULLITE TPS TEST PANEL COMPONENTS

TPS mass:		
Tiles, kg/m^2	6.93	
Gap filler, kg/m^2	0.54	
Strain isolator, kg/m^2	4.98	
Total TPS mass, kg/m^2		12.45
Primary structure mass:		
Skin, kg/m^2	4.49	
Stiffeners, kg/m^2	7.42	
Clips, kg/m^2	0.20	
Stringers, kg/m^2	2.15	
Rivets, kg/m^2	0.10	
Total primary structure mass, kg/m^2		14.36
Total test panel mass, kg/m^2		26.81

TABLE II.- TEST SEQUENCE AND TEST CONDITIONS FOR MULLITE PANEL

Test	Heat source (a)	Radiant heat			Delay time, s	Aerodynamic heat			
		Heatup time, s	Constant-temperature time, s	Constant temperature, K		Time in stream, s	Temperature in stream, K	Δp, kPa	α, deg
1	[b]R	330	410	990					
2	[b]R	340	1000	1010					
3	R	340	30	1110					
4	R	310	205	1230					
5	R	360	520	1220					
6	R & A	370	443	1140	14	21	1190	13.8	13
7	R	370	130	1130					
8	R	360	450	1140					
9	R	360	575	1200					
10	R	390	285	1180					
11	R	370	425	1190					
12	R & A	370	408	1190	7	37	1200	10.3	15
13	R & A	370	438	1190	6	41	1210	11.4	15
14	R & A	360	409	1180	7	35	1220	11.2	15
15	[b]R	370	765	1210					
16	R & A	380	659	1190	8	13	1190	11.6	15
17	[b]R	350	1285	1180					
18	R & A	380	625	1180	9	41	1230	11.7	15
19	R & A	360	670	1180	9	34	1210	11.7	15
20	R & A	360	686	1180	10	41	1220	11.4	15
21	R & A	360	629	1190	8	41	1210	11.4	15

[a] R is radiant heat; R & A is radiant and aerodynamic heat.

[b] Controlled cooldown at 2 K/s instead of natural cooldown of figure 10.

TABLE III.- FLOW CONDITIONS FOR AERODYNAMIC HEATING TESTS OF MULLITE PANEL

Test	Free stream					Local			
	T_t, K	R_∞, m^{-1}	q_∞, kPa	M_∞	p_∞, kPa	R_l, m^{-1}	q_l, kPa	M_l	p_l, kPa
6	1890	4.67×10^6	63.6	6.8	2.00	8.37×10^6	189.6	4.35	14.8
12	1860	4.63	61.9	6.7	1.99	8.76	203.4	4.17	17.2
13	1860	4.68	62.5	6.7	2.01	8.99	209.6	4.17	17.7
14	1860	4.63	61.9	6.7	1.99	8.82	205.5	4.17	17.4
16	1860	4.73	63.4	6.7	2.04	9.02	210.3	4.17	17.8
18	1890	4.63	62.9	6.8	1.98	8.82	212.4	4.17	17.9
19	1890	4.60	62.6	6.8	1.97	8.89	213.7	4.17	18.1
20	1910	4.44	60.9	6.8	1.90	8.82	213.0	4.17	18.1
21	1860	4.63	61.9	6.7	1.99	8.92	207.5	4.17	17.6

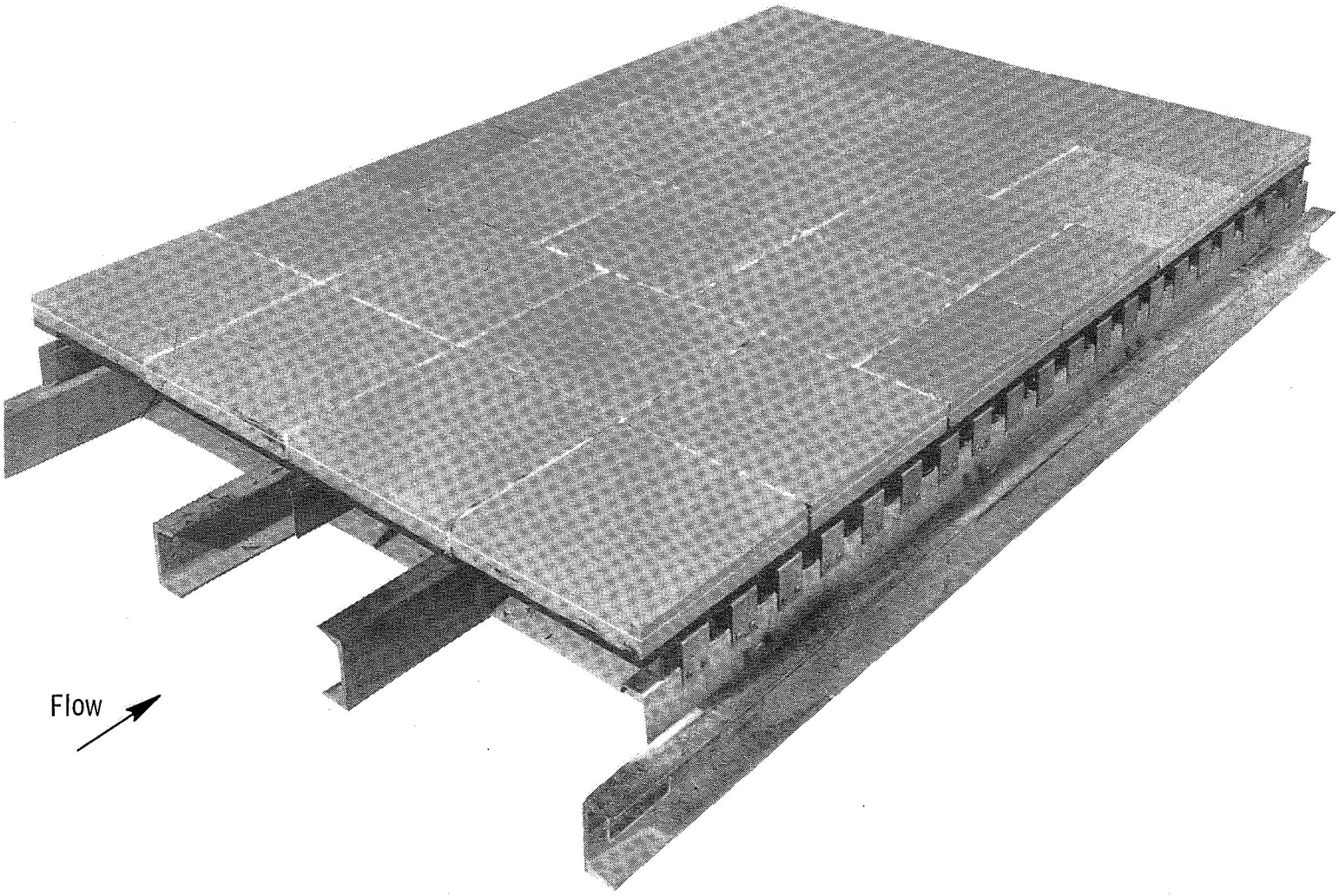

L-72-3372.1

Figure 1.- Test panel with mullite tiles.

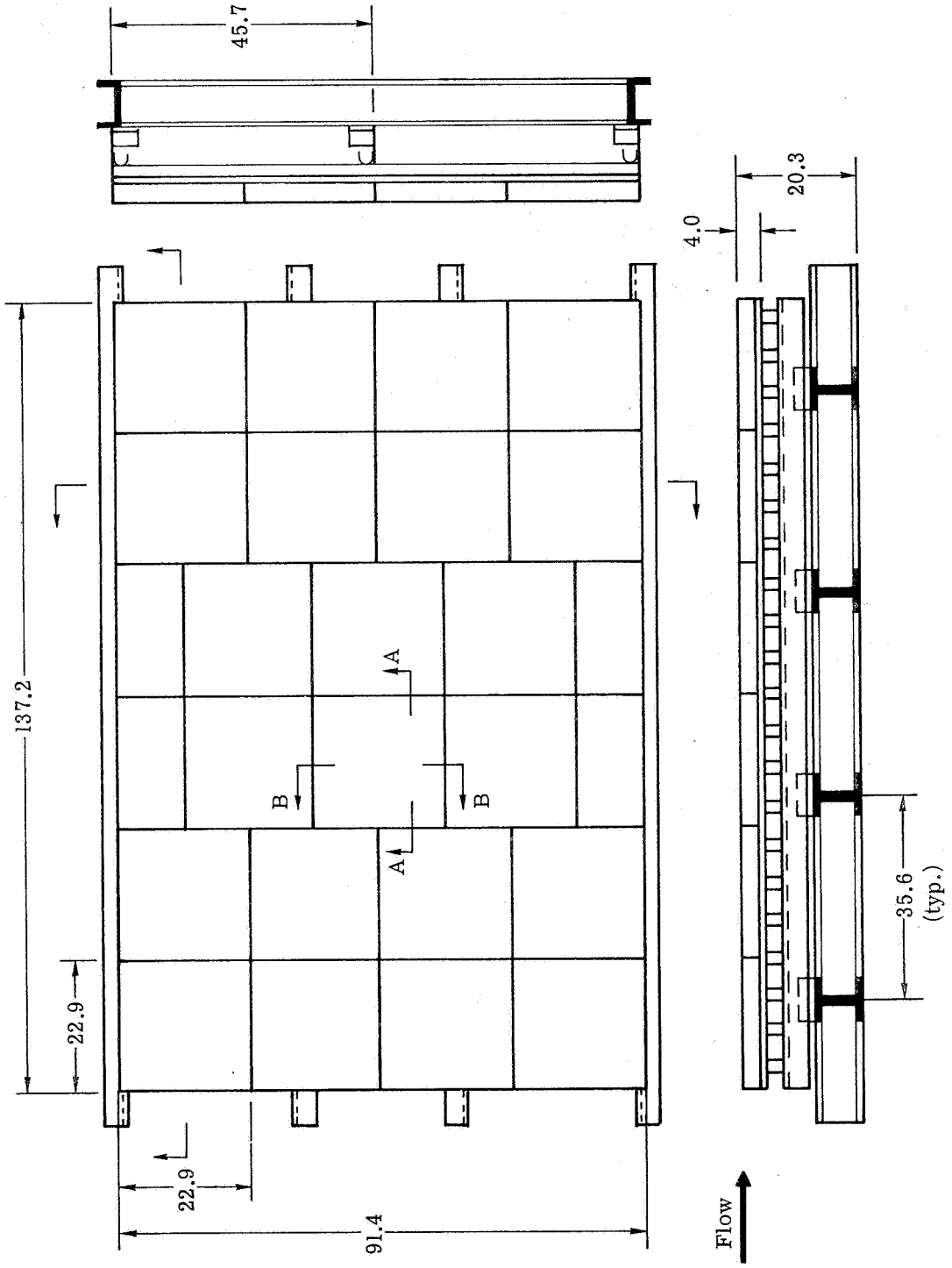

(a) Test panel assembly.

Figure 2.- Mullite test panel details. (All dimensions are in centimeters.)

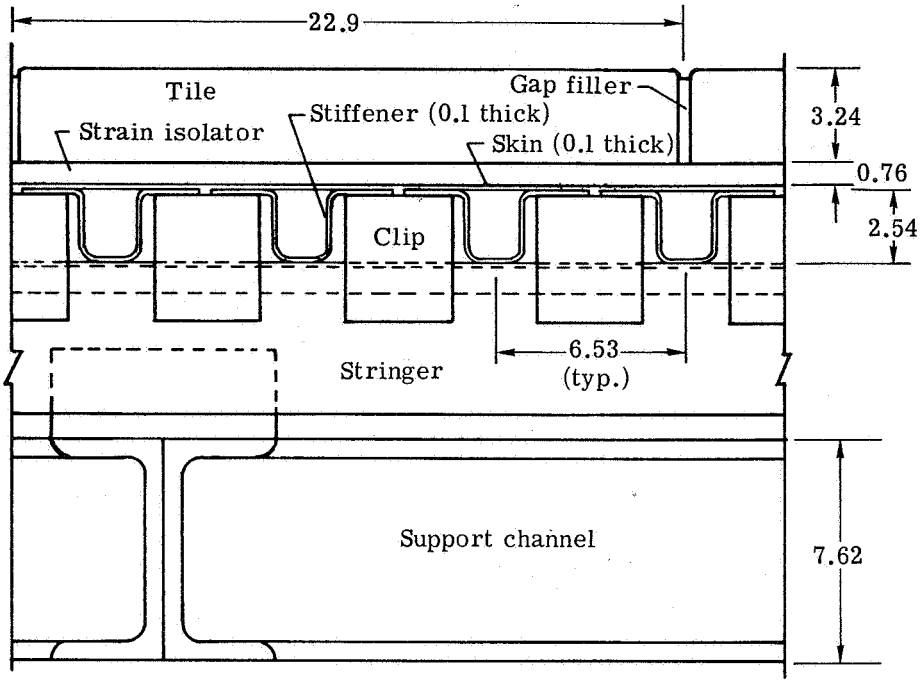

(b) Section A-A.

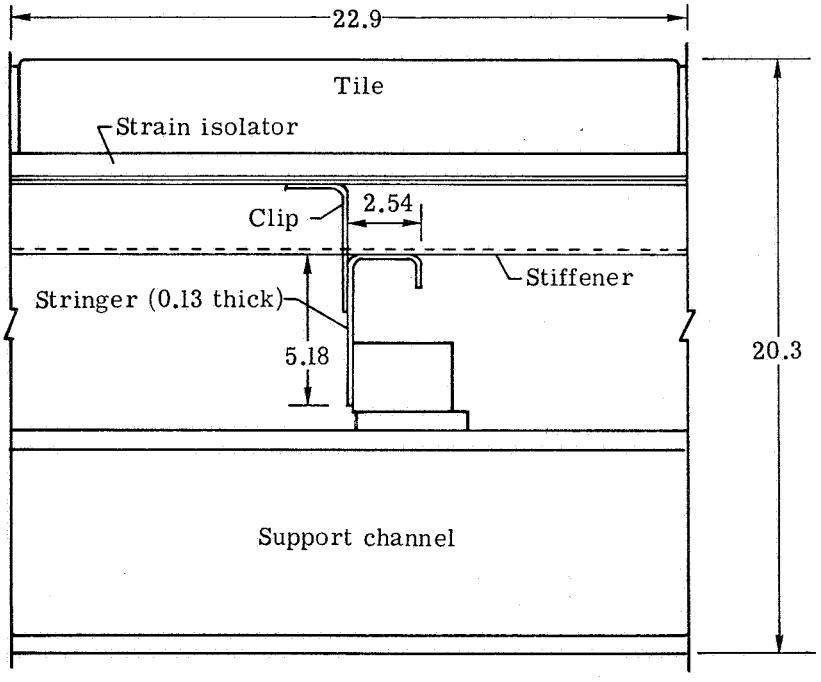

(c) Section B-B.

Figure 2.- Concluded.

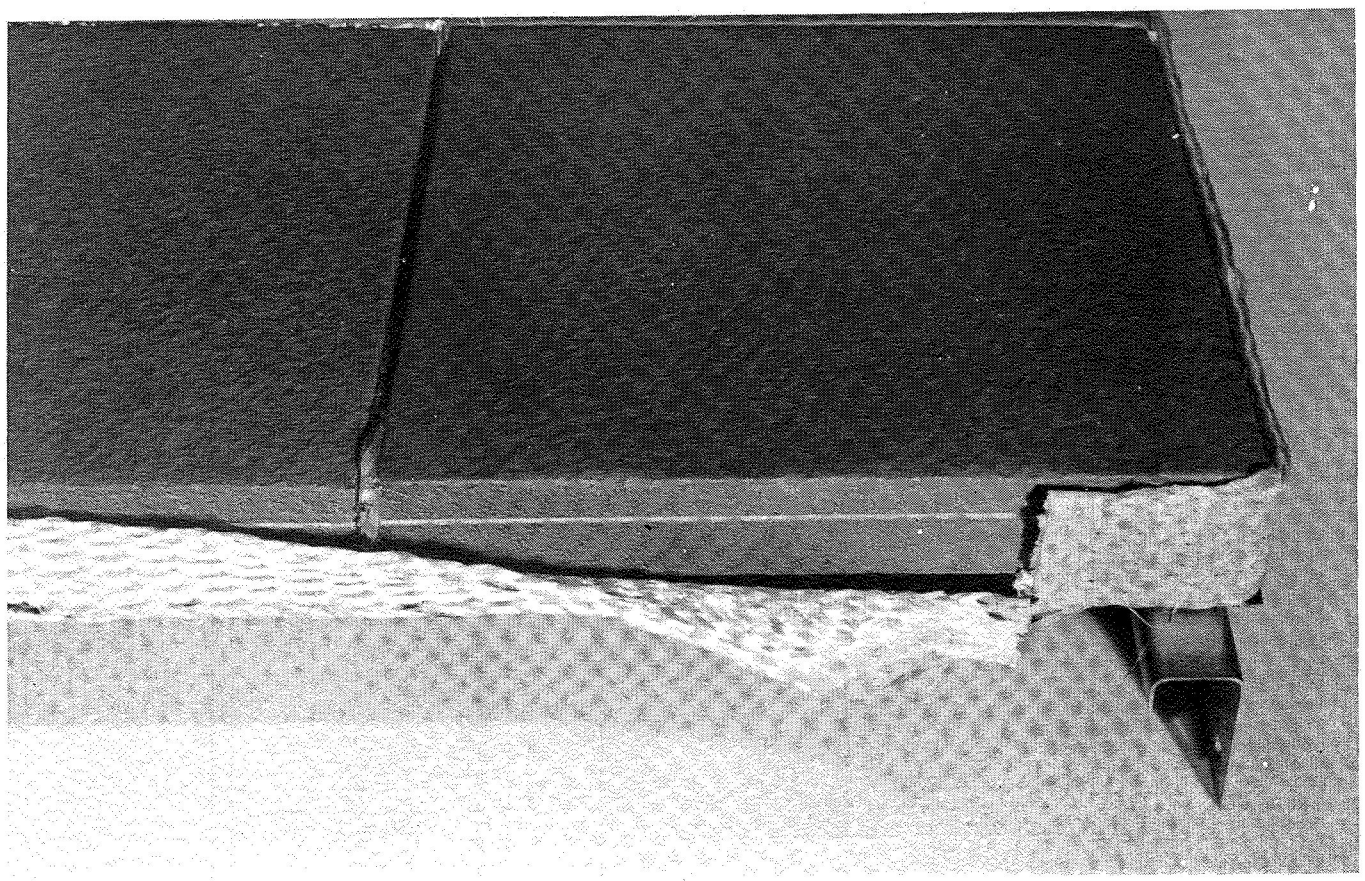

L-72-3293

Figure 3.- Omniweave gap filler around edge of tile.

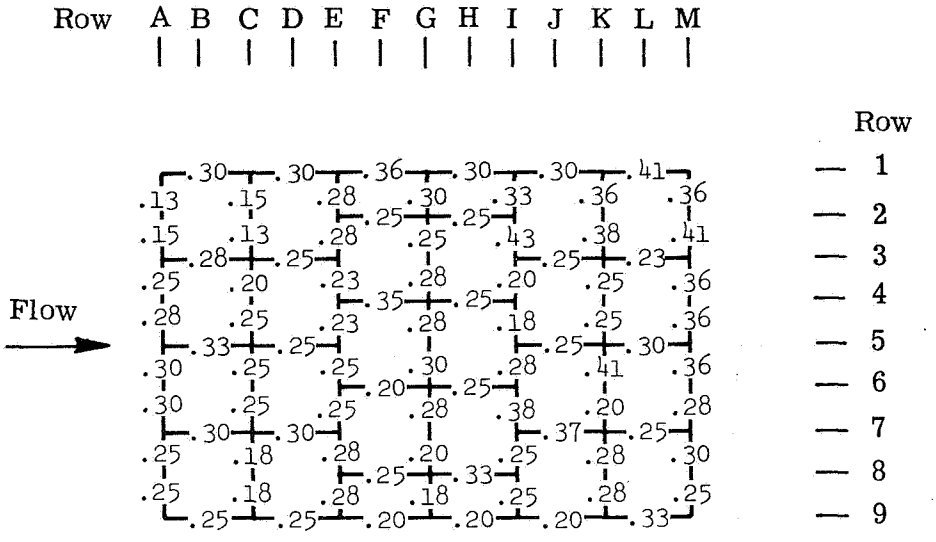

(a) Gap width in centimeters.

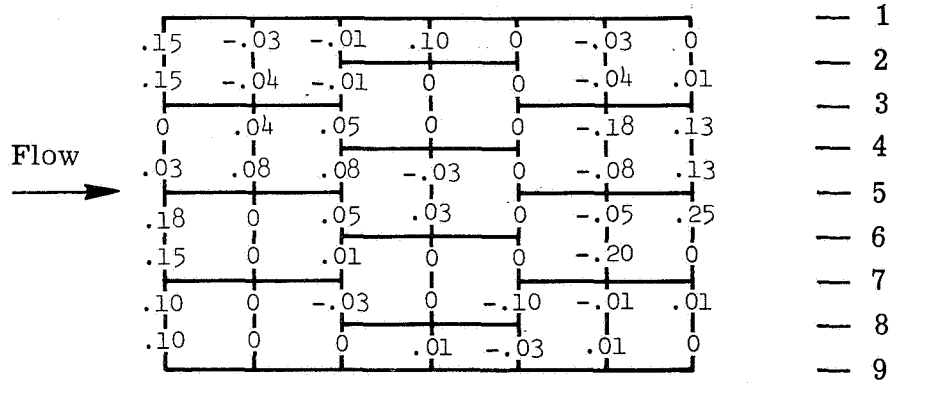

(b) Step height (rearward-facing step is negative) in centimeters.

Figure 4.- Variation in tile gap geometry.

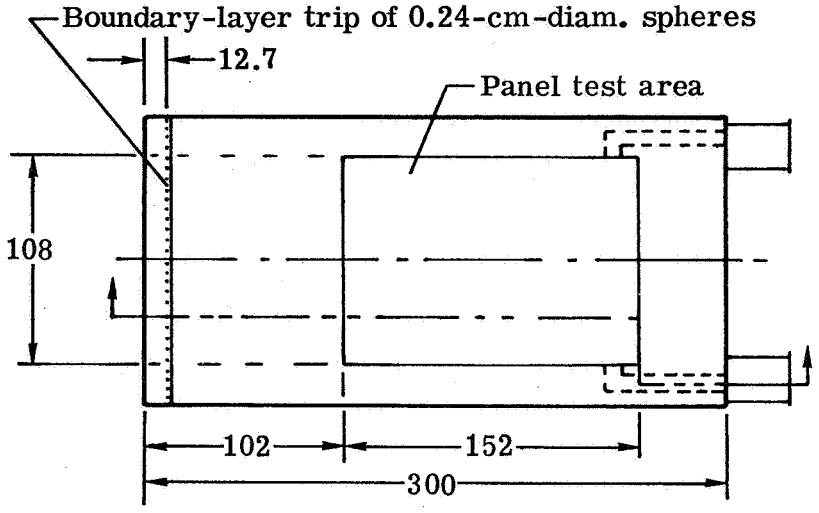

(a) Plan view.

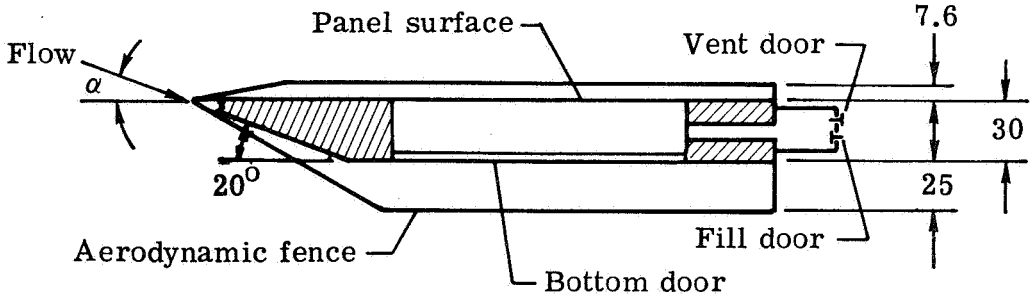

(b) Longitudinal cross section.

Figure 5.- Details of panel holder. (Dimensions are in centimeters unless otherwise indicated.)

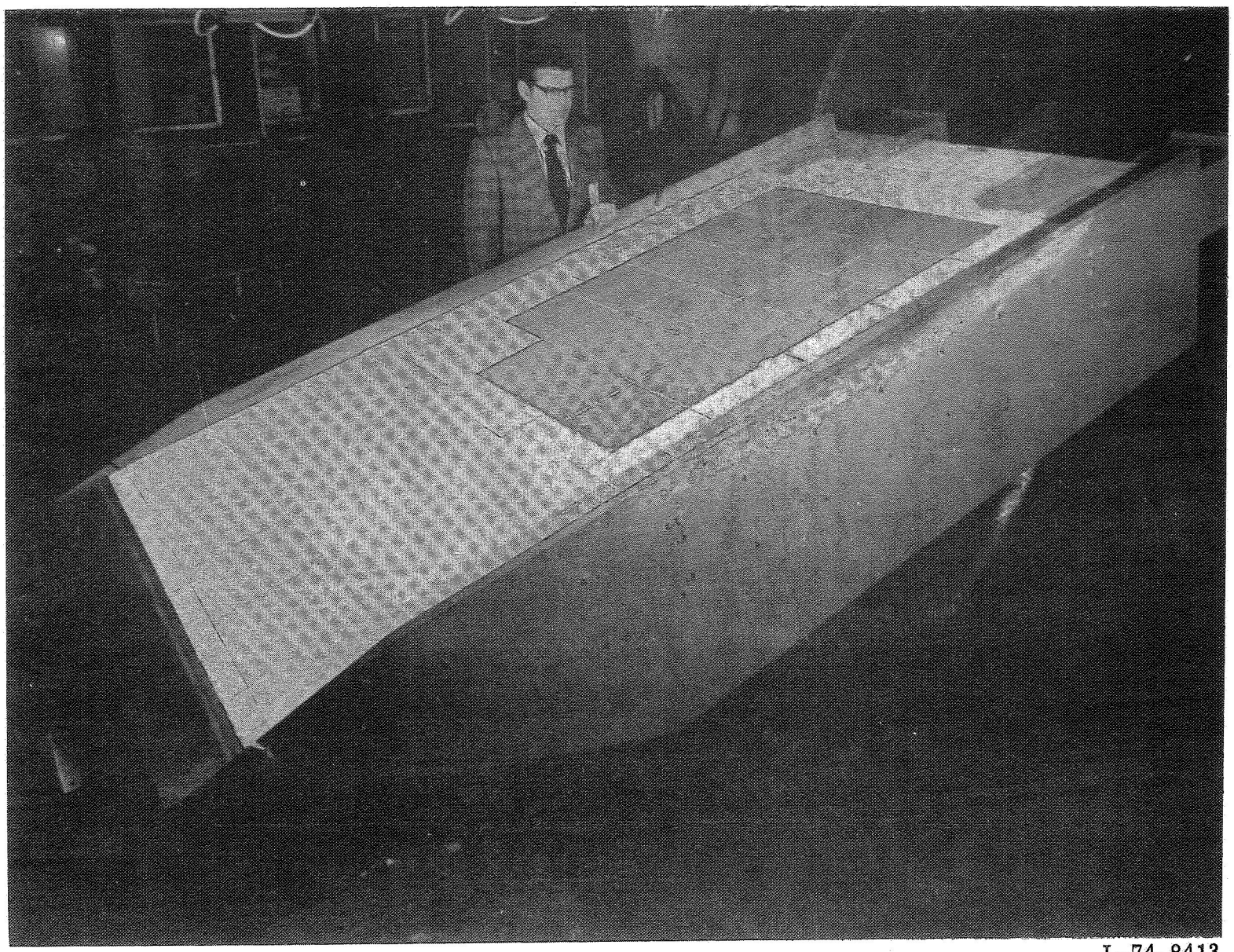

L-74-8413

Figure 6.- Test panel installed in Langley 8-foot high-temperature structures tunnel.

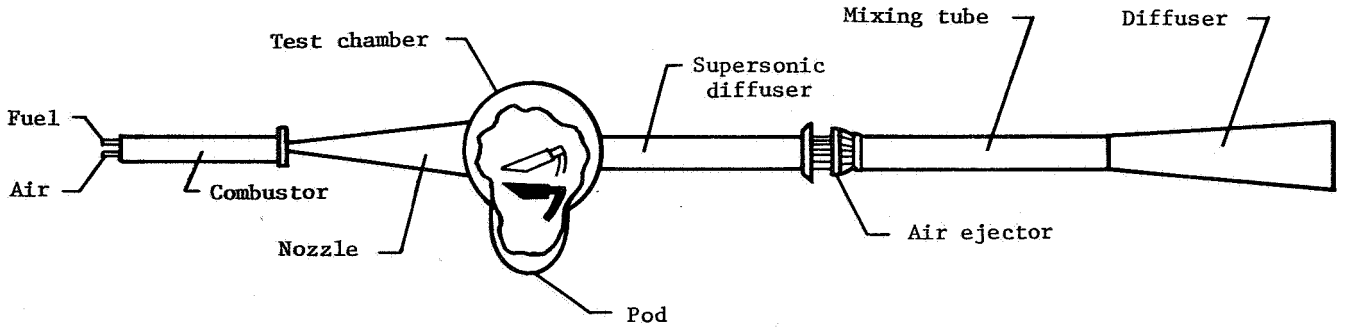

Figure 7.- Langley 8-foot high-temperature structures tunnel.

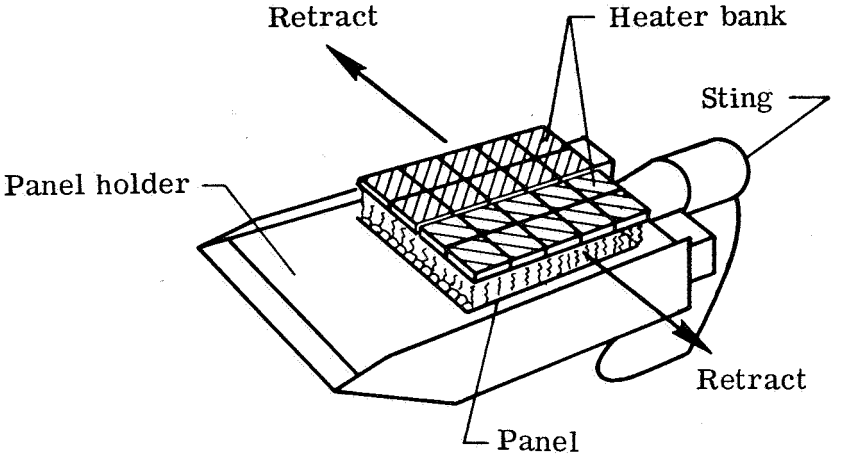

(a) Radiant heaters without acoustic covers.

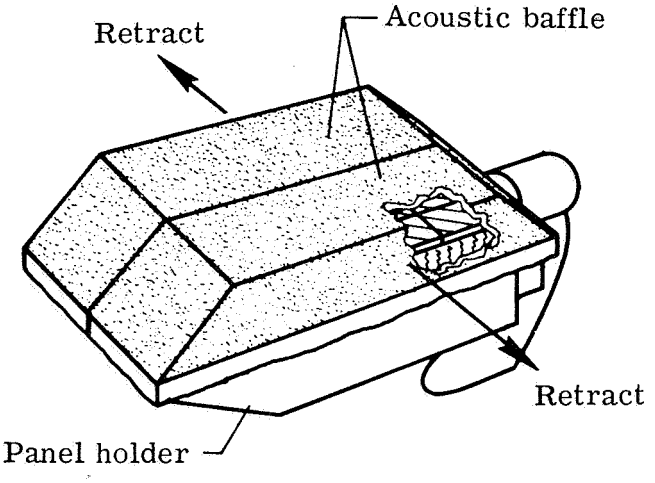

(b) Radiant heaters with acoustic covers.

Figure 8.- Retractable radiant heaters with and without acoustic covers.

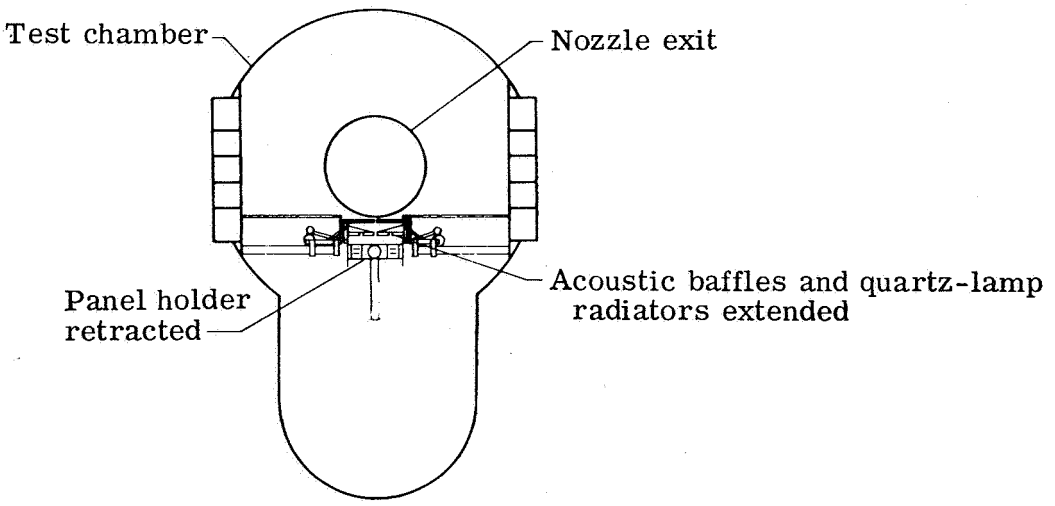

(a) Pretest and posttest.

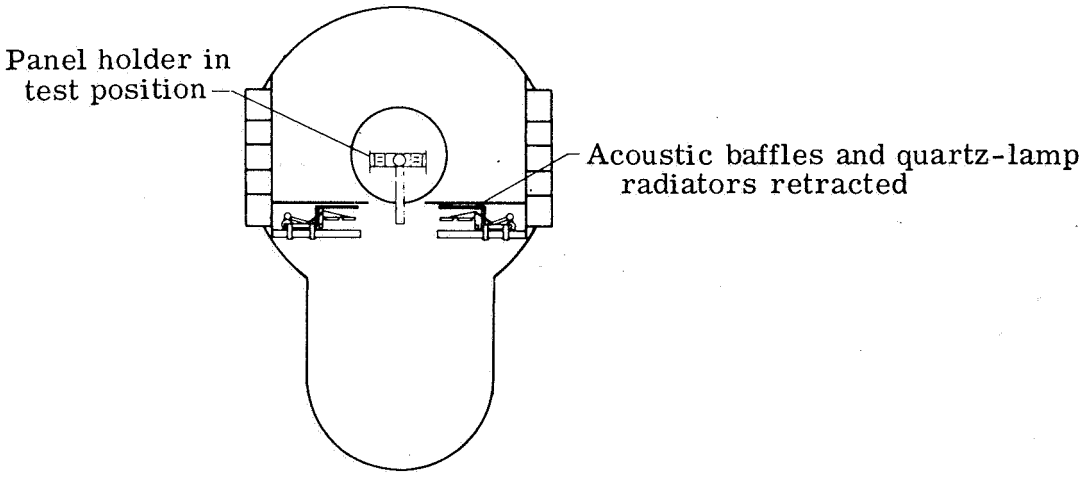

(b) During test.

Figure 9.- Cross-sectional views of test section.

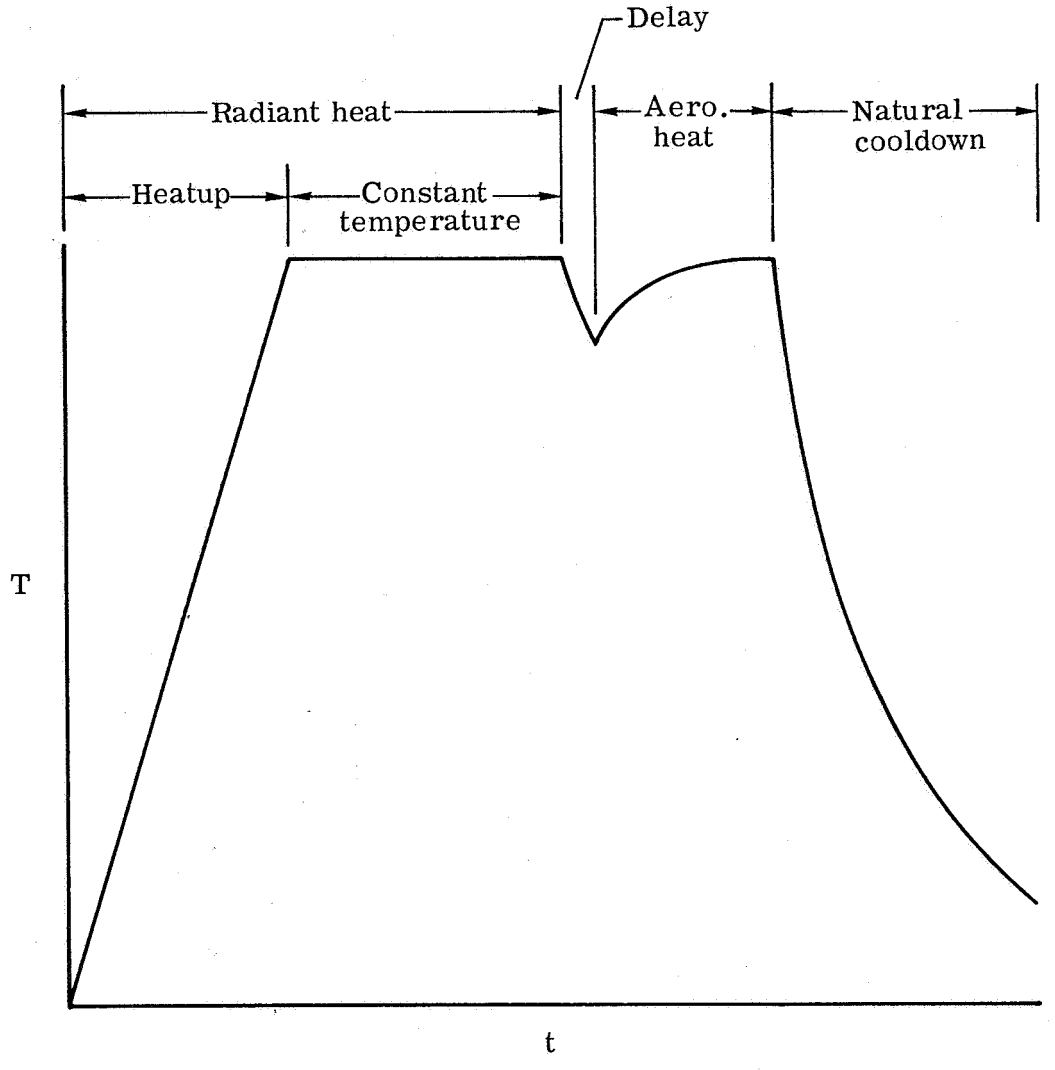

Figure 10.- Typical radiant-heat—aerodynamic-heat cycle.

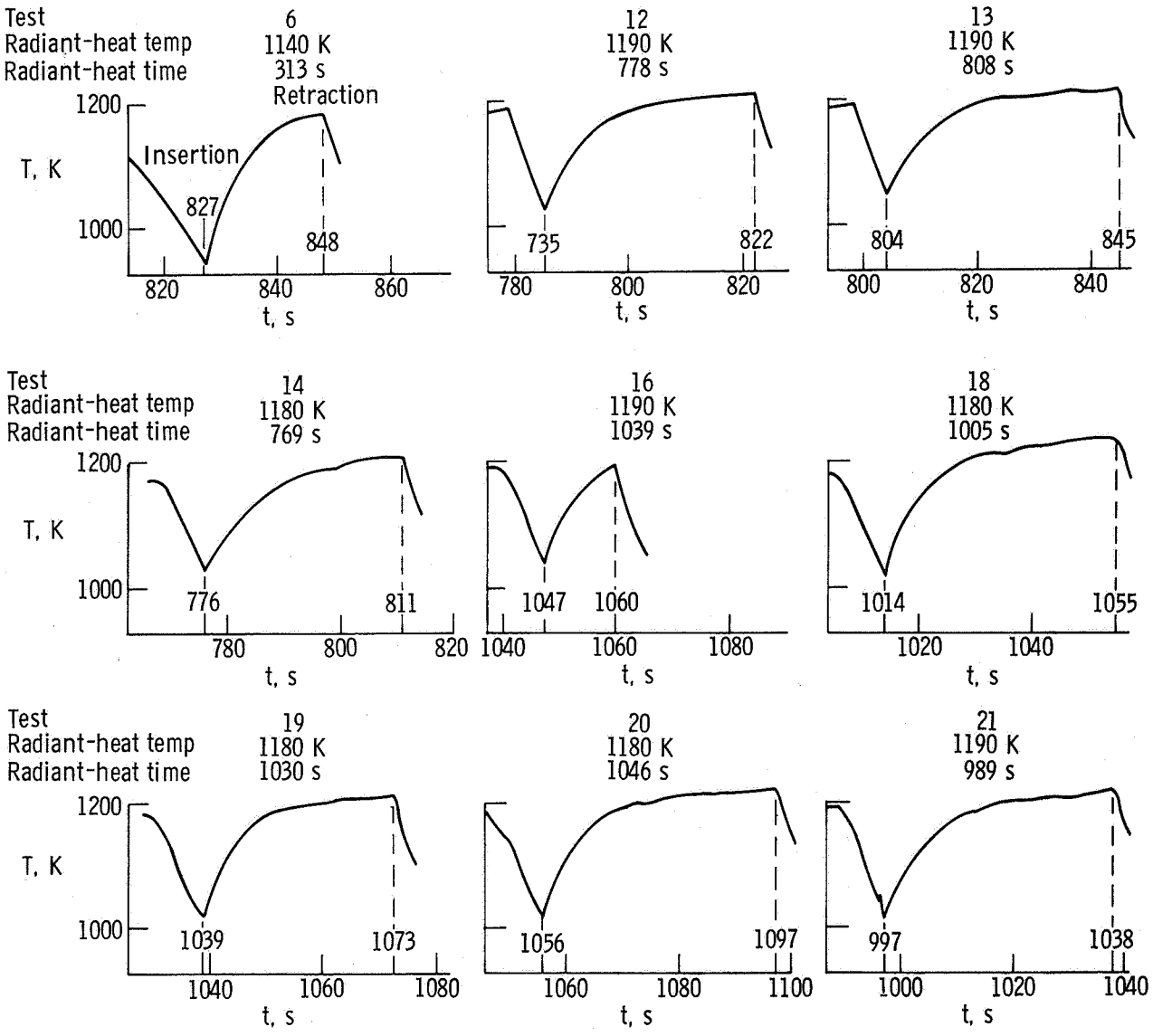

Figure 11.- Surface temperature histories of each aerodynamic heating test of the mullite panel. (See table II.)

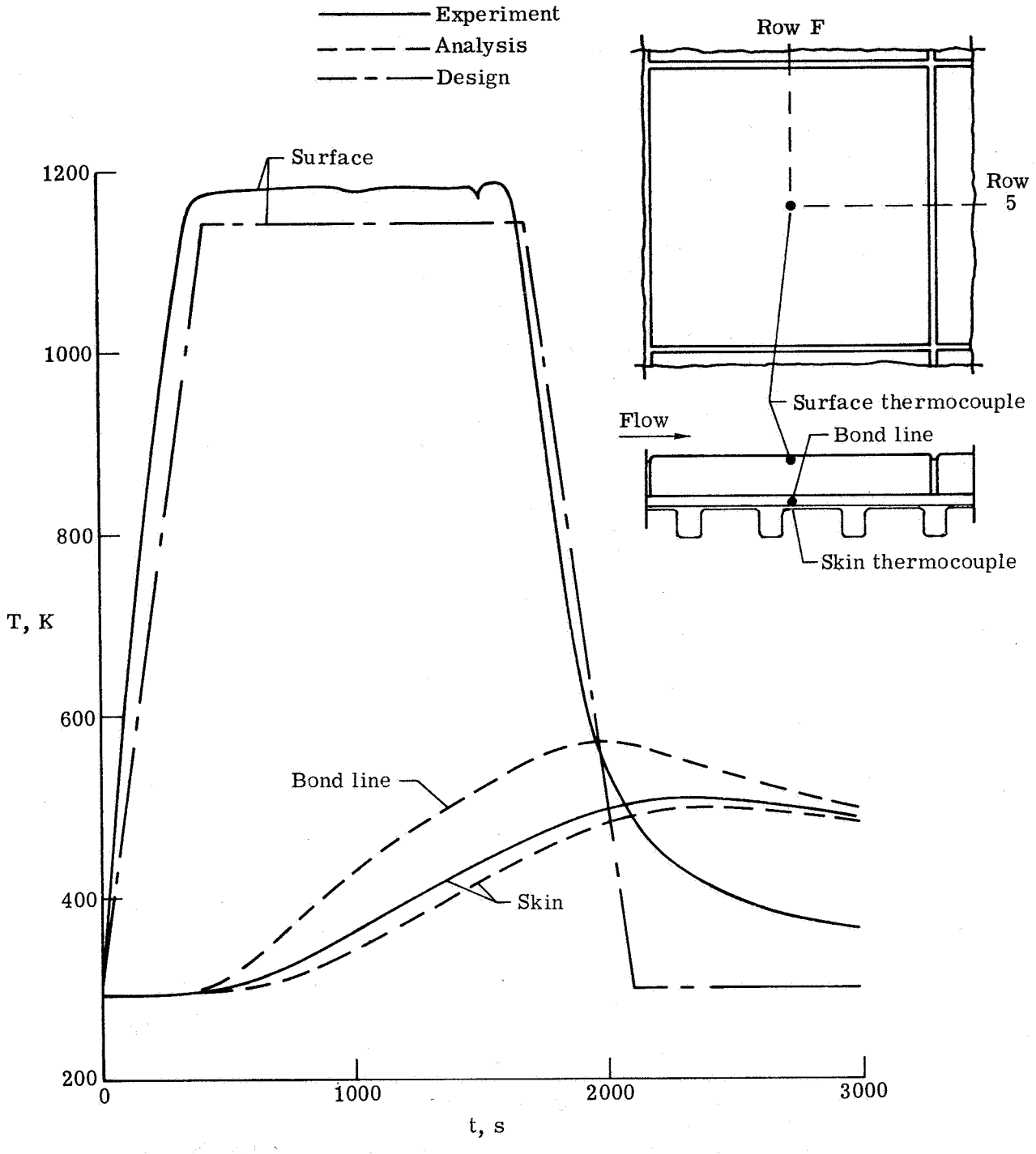

Figure 12.- Thermal response of mullite TPS to a radiant-heat cycle (test 17).

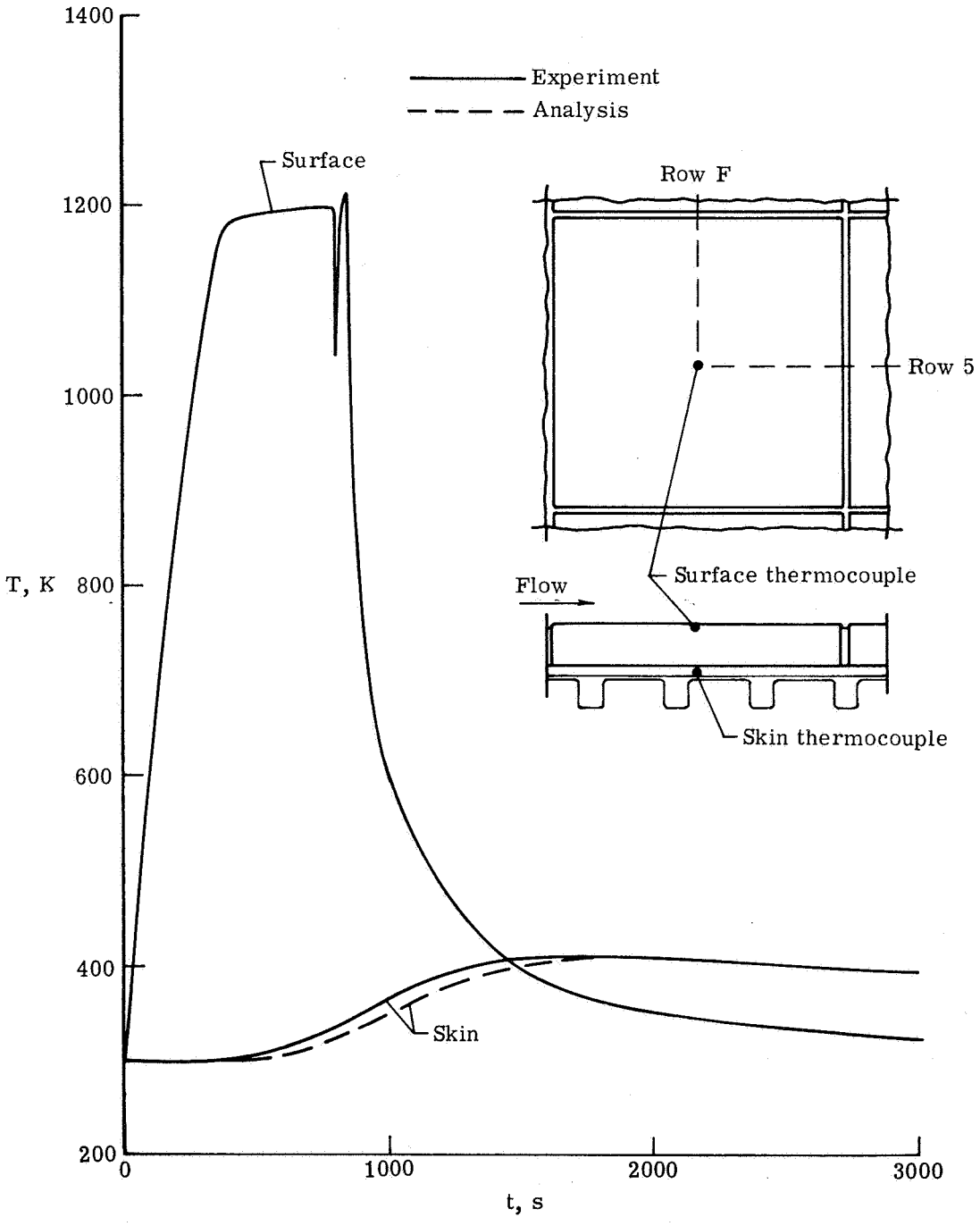

(a) Entire heat cycle.

Figure 13.- Thermal response of mullite TPS to a radiant-heat—aerodynamic-heat cycle (test 13).

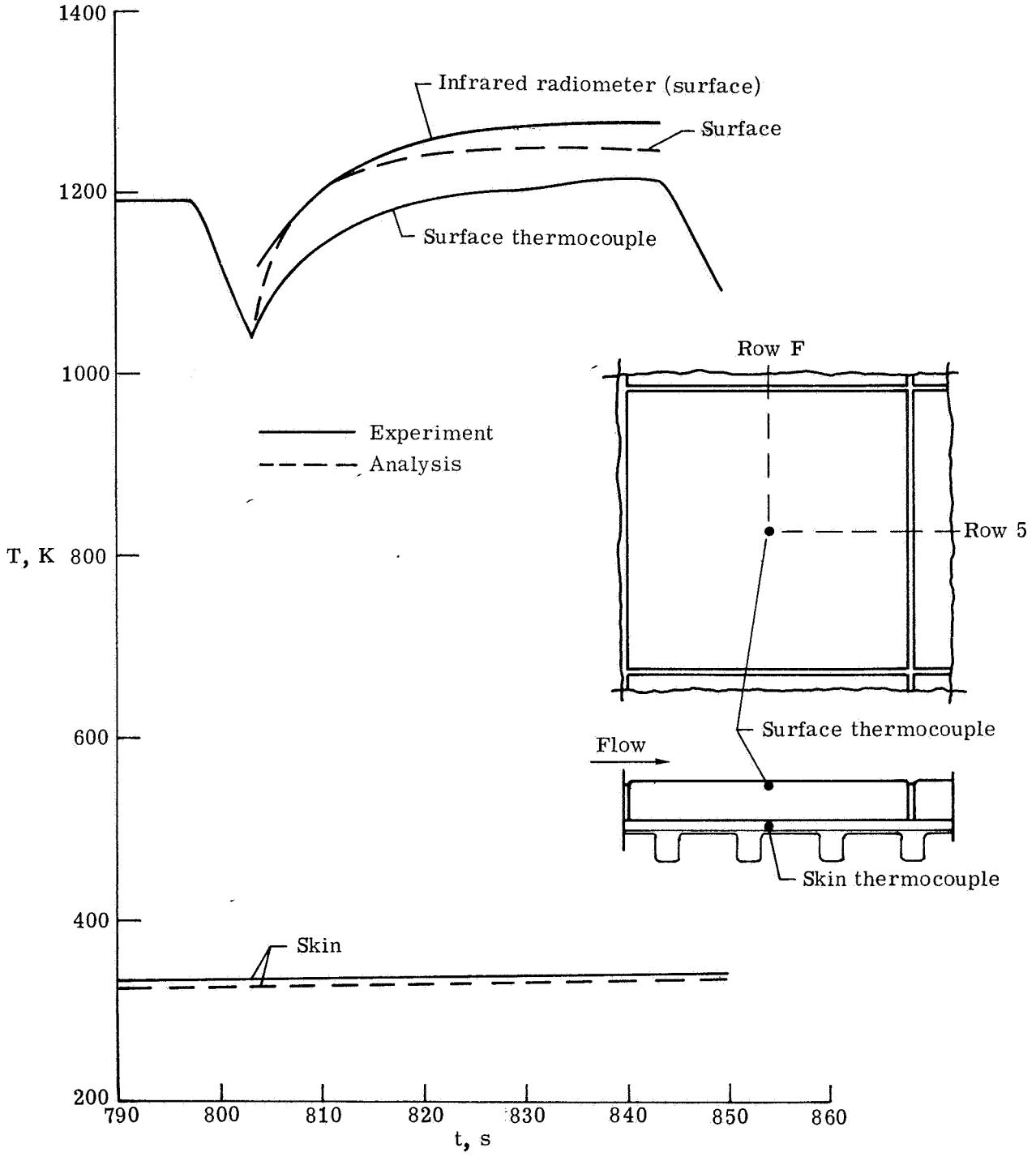

(b) Aerodynamic-heat cycle.

Figure 13.- Concluded.

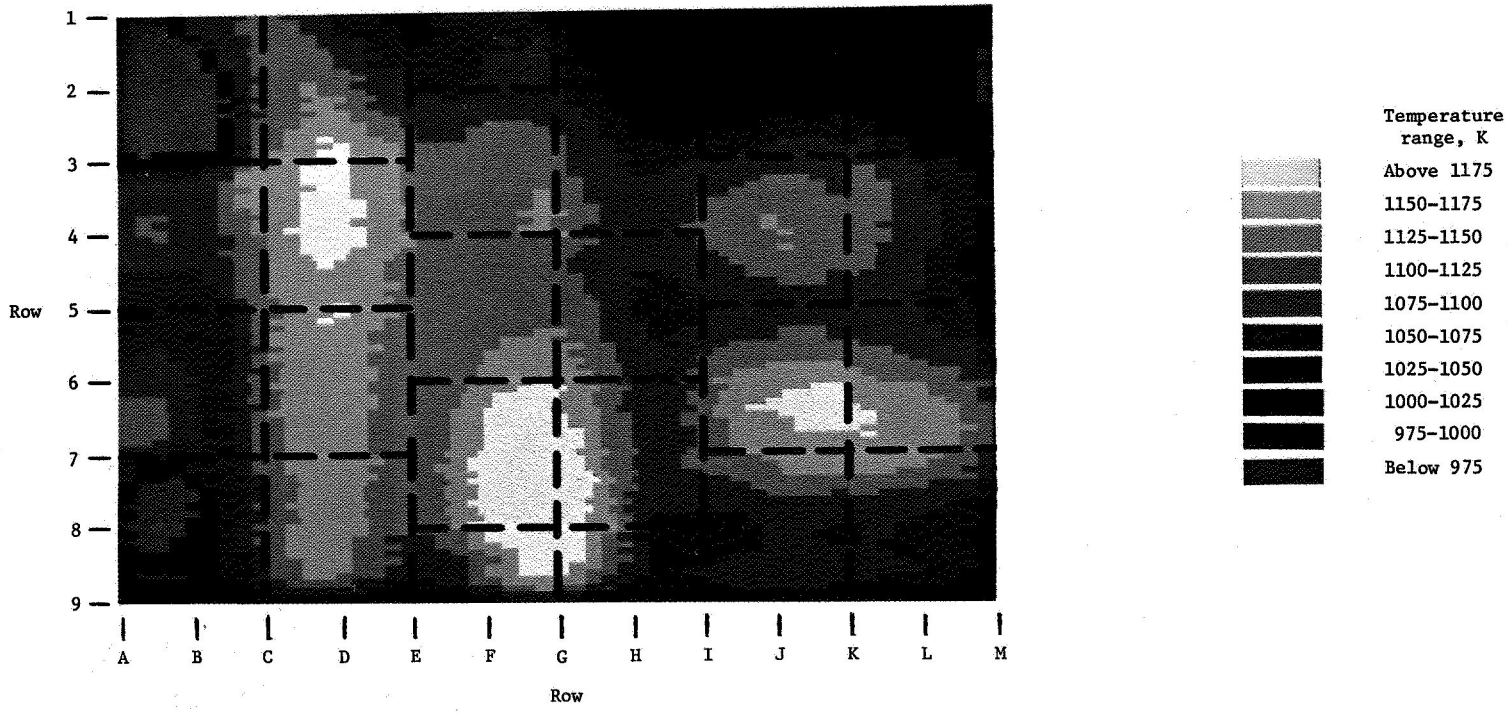

(a) After radiant heating.

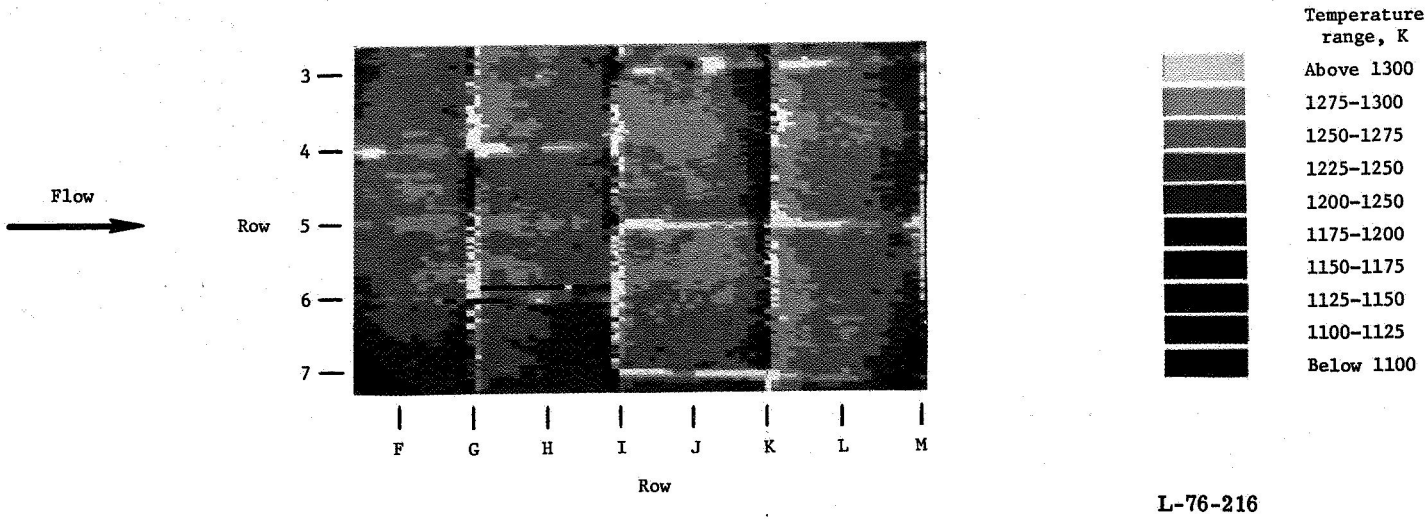

(b) During aerodynamic heating (840 to 843 s).

Figure 14.- Surface temperature distribution on mullite panel for test 13 from infrared radiometer.

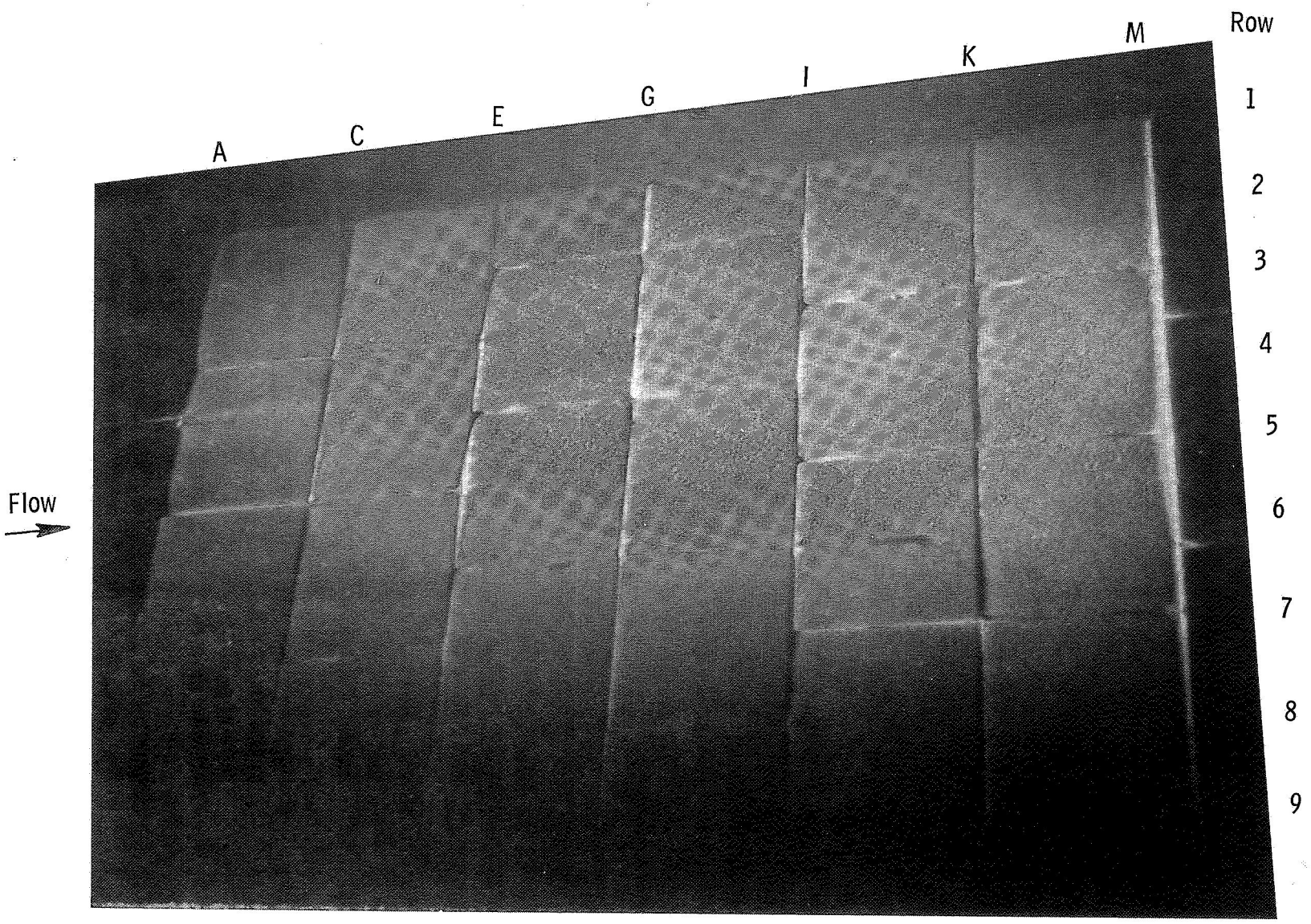

Figure 15.- Hot panel during aerodynamic heating of test 18.

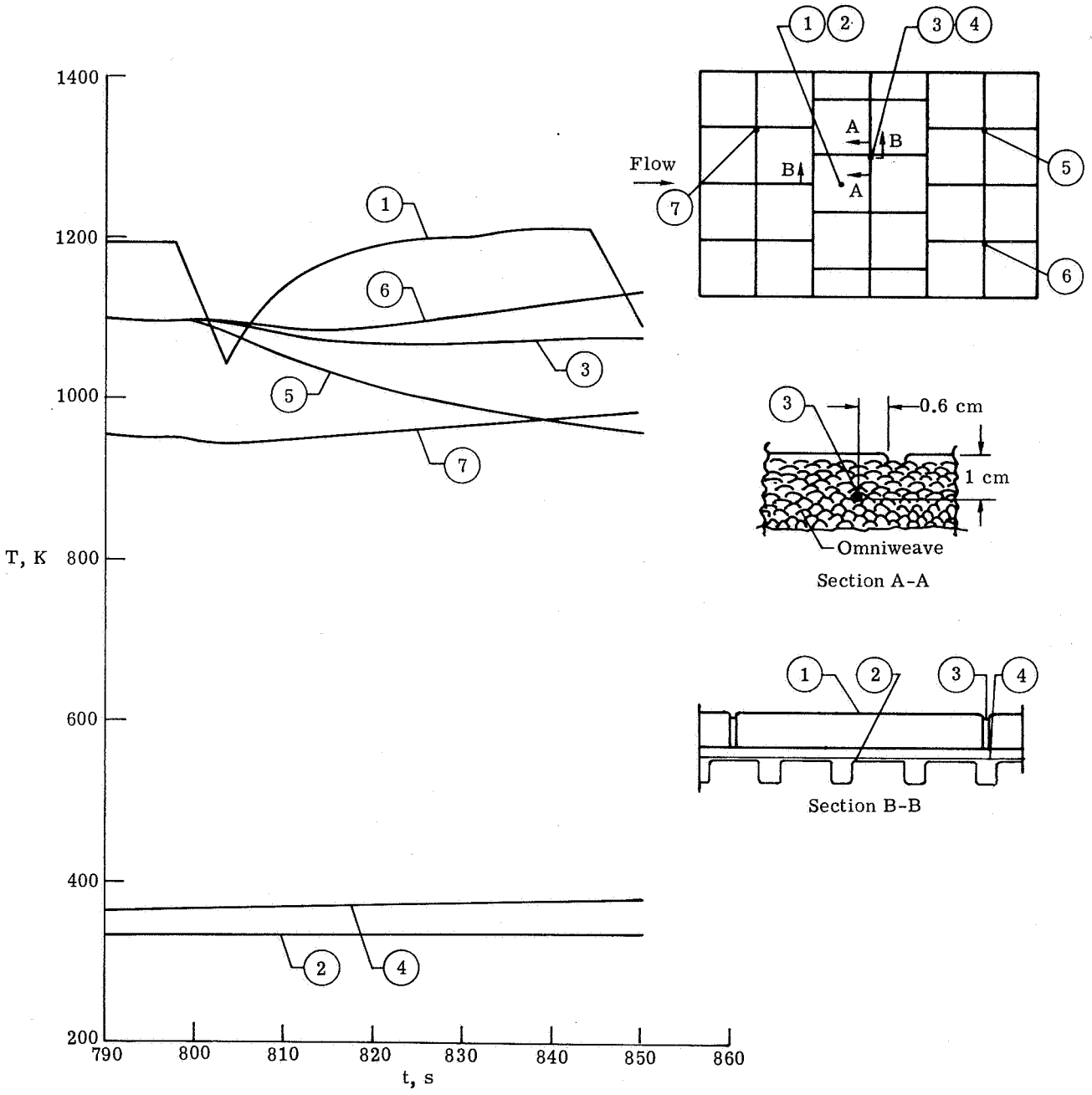

Figure 16.- Thermal response of mullite TPS at tile edges (test 13).

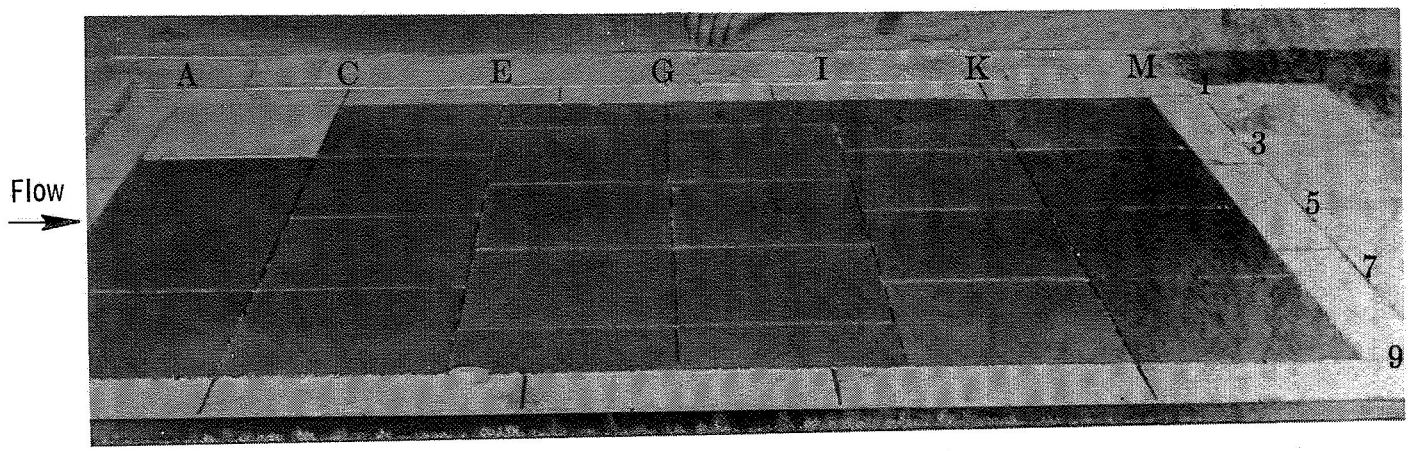

(a) Before test 4.

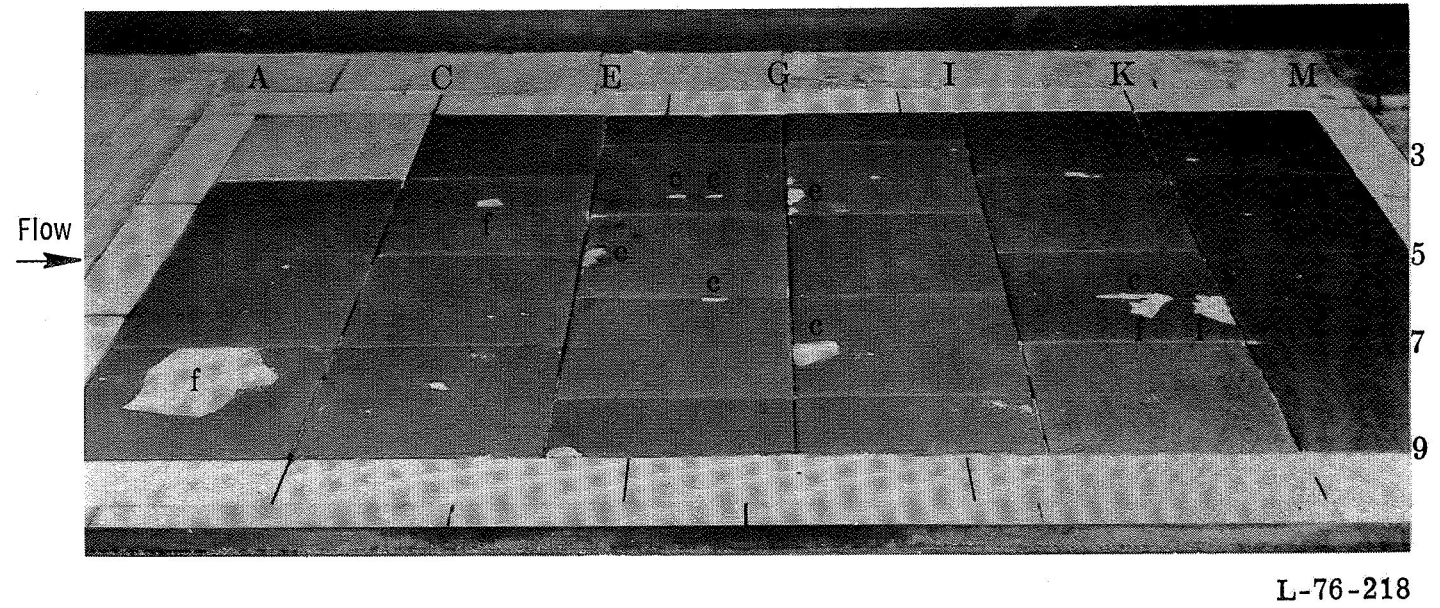

(b) After test 21.

Figure 17.- Surface appearance of panel before and after tests.

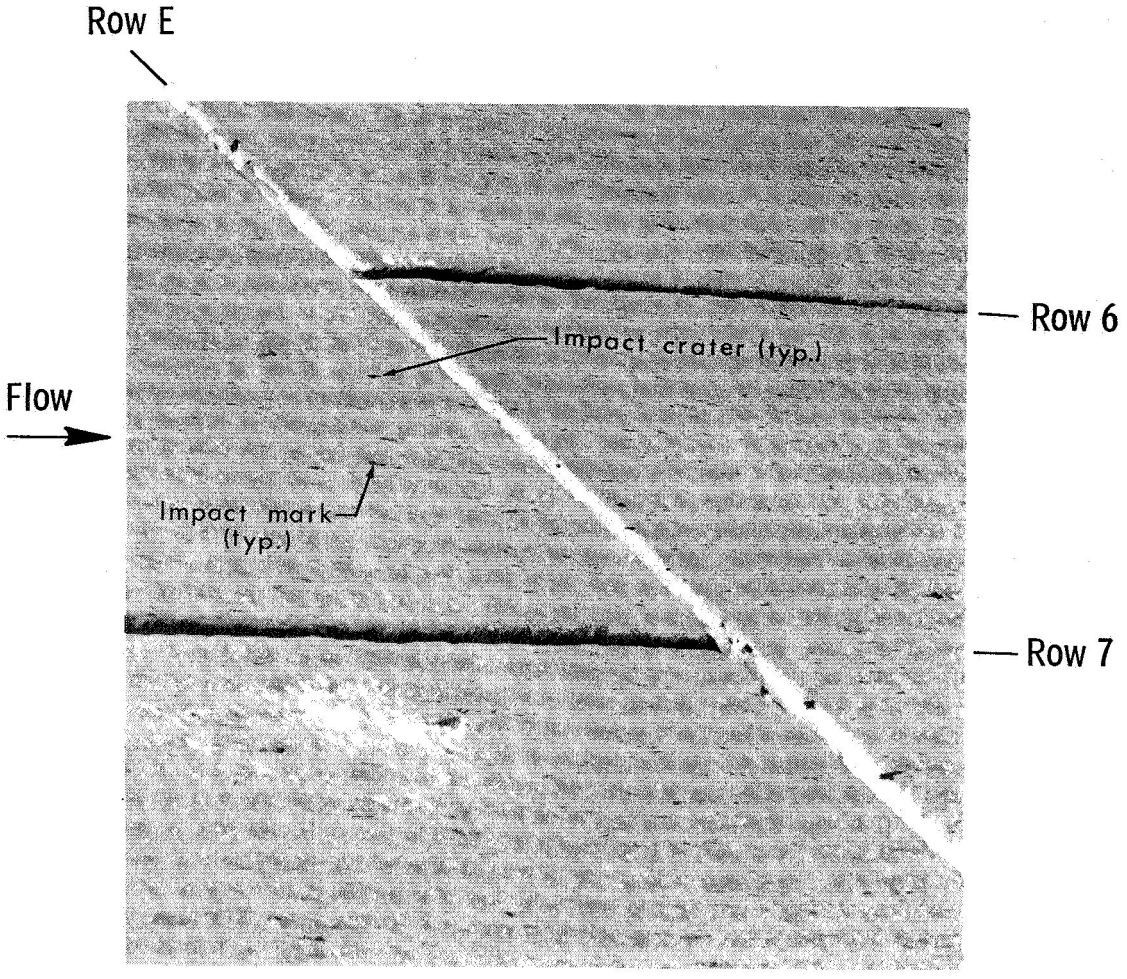

L-76-219

Figure 18.- Surface damage produced by particle impact.

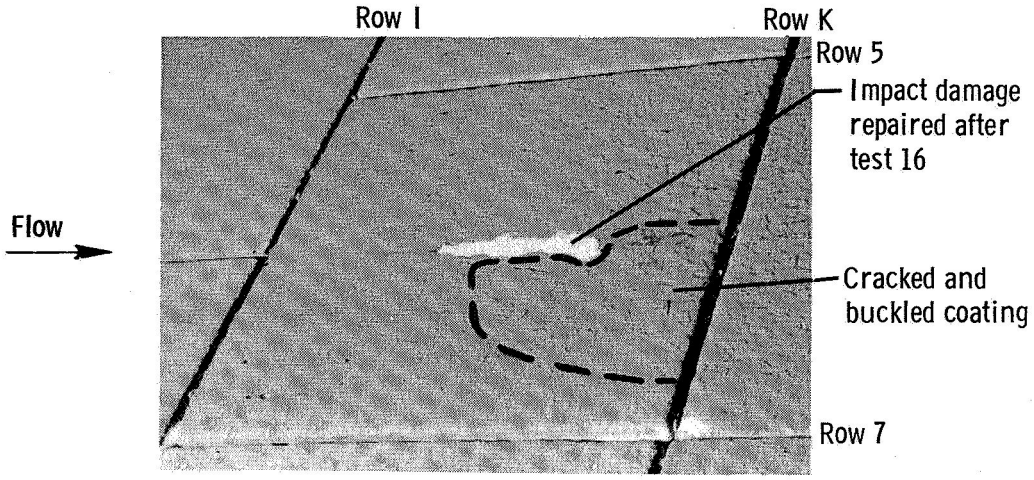

(a) Posttest 19.

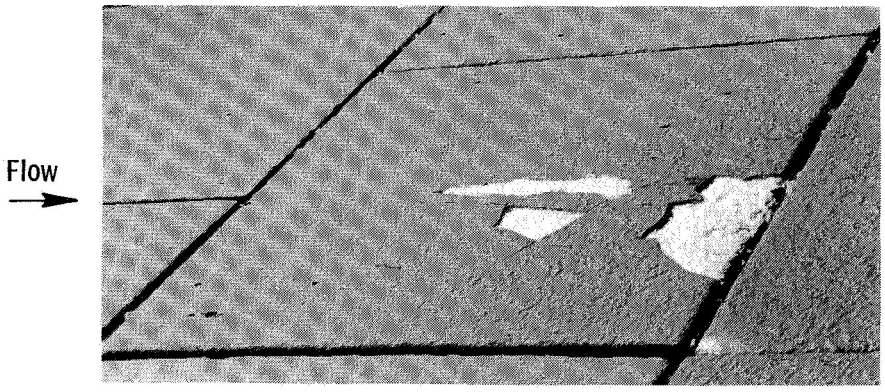

(b) Posttest 20.

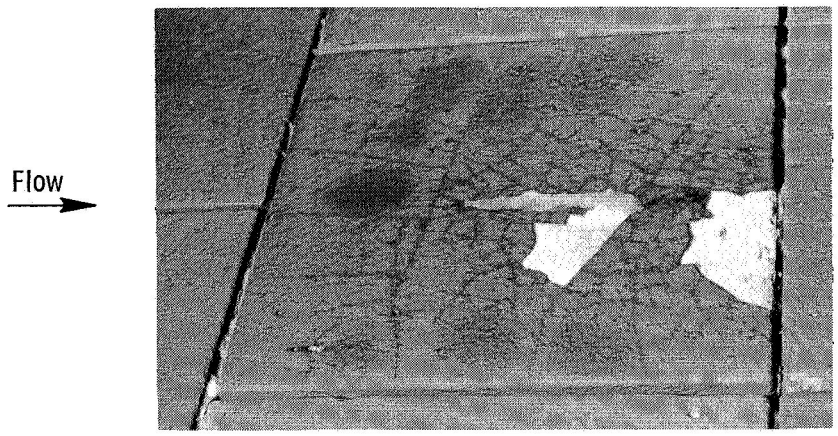

(c) Posttest 21.

L-76-220

Figure 19.- Cracking and flaking of coating.

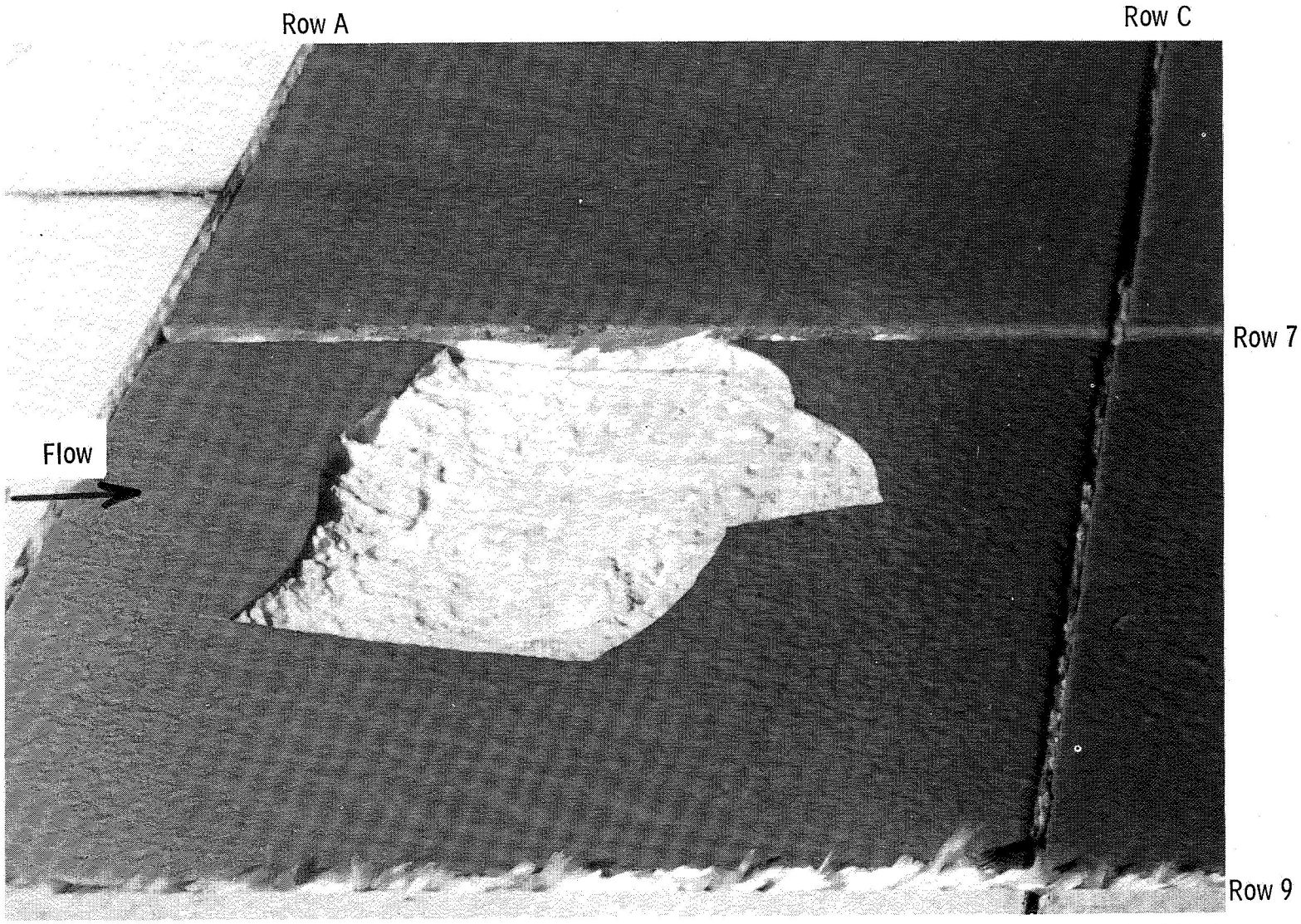

Figure 20.- Tile failure during test 6.

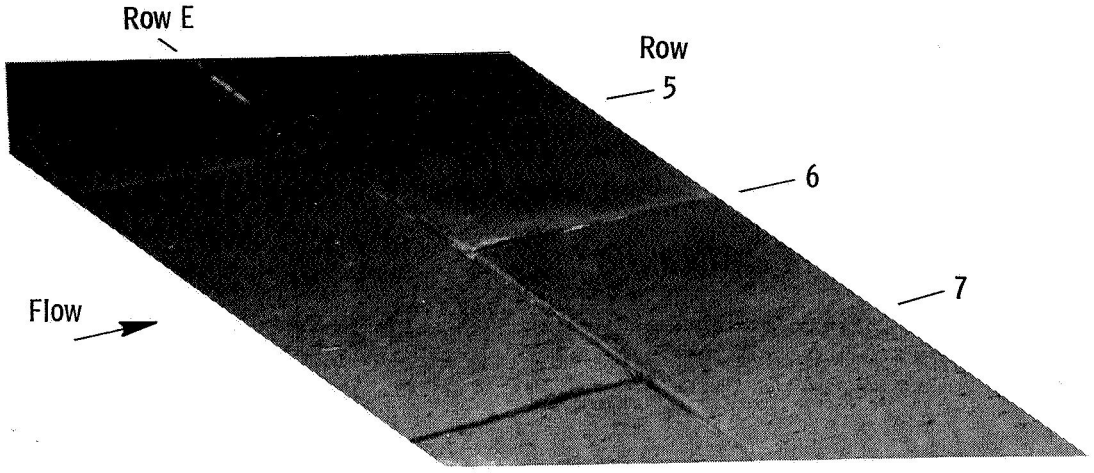

(a) Posttest 13.

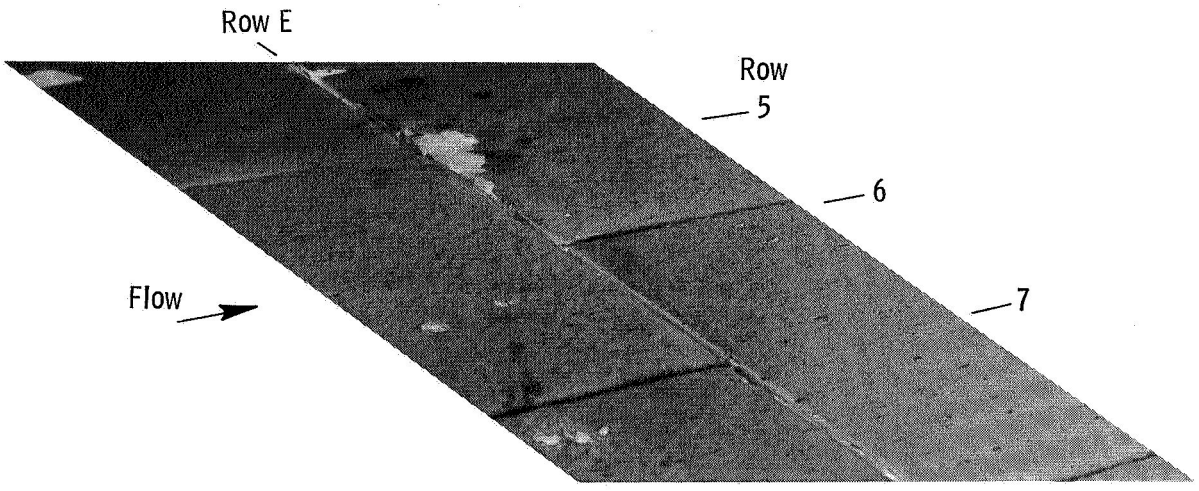

(b) Posttest 21.

L-76-221

Figure 21.- Erosion of forward-facing step.

U.S. Government Printing Office: 1976—638-921 Region No. 3-II

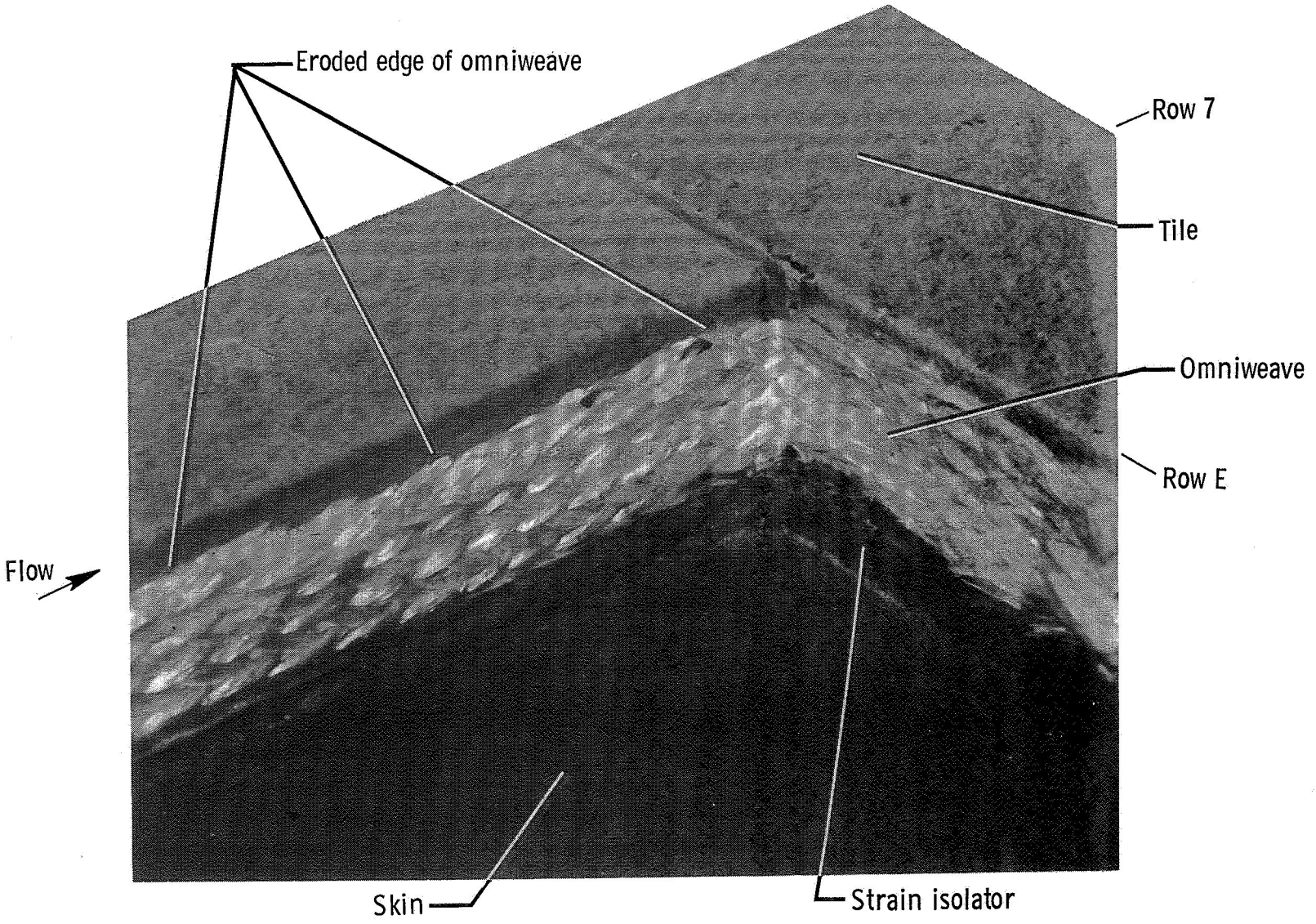

Figure 22.- Cross section of omniweave gap filler after test 21.